

# Classifying Urban Regions by Aggregated Pollutant–Weather Correlation Strength: A Spatiotemporal Study

Koyena Ghosh<sup>1†</sup>, Suchismita Banerjee<sup>2\*†</sup>, Urna Basu<sup>2</sup>, Banasri Basu<sup>3</sup>

<sup>1</sup>Maulana Abul Kalam Azad University of Technology, West Bengal, 741249, India.

<sup>2</sup>S. N. Bose National Centre for Basic Sciences, Kolkata, 700106, India.

<sup>3</sup>Indian Statistical Institute, Kolkata, 700108, India.

\*Corresponding author(s). E-mail(s): [suchib@bose.res.in](mailto:suchib@bose.res.in);

†These authors contributed equally to this work.

## Abstract

Understanding pollutant–meteorology interactions is essential for environmental risk assessment. This study develops an entropy-based statistical framework to analyze static and temporal dependencies between urban air pollutants and meteorological variables across multiple Indian cities. Dependence is quantified using complementary linear and nonlinear measures, including Pearson correlation, mutual information, and relative conditional entropy. A key methodological contribution is a PCA-based composite indexing framework that integrates these heterogeneous metrics into a unified and interpretable correlation score. For each pollutant–meteorological pair within a city, PCA is used to extract a joint variability index, while spatial variability is assessed by aggregating correlations across cities. These indices are further combined to derive a comprehensive city-level correlation score that represents overall pollutant–meteorology coupling strength and enables classification of cities into distinct interaction regimes. Sensitivity analysis, performed by systematically excluding individual variable pairs, demonstrates the robustness of the framework, with no single pair exerting disproportionate influence. Temporal dependencies are examined using transfer entropy and time-delayed mutual information. Results indicate that relative humidity generally leads changes in pollutant concentrations, whereas ambient temperature tends to lag, highlighting contrasting causal influences. Mutual information peaks at zero lag and decays rapidly, indicating strong short-term interactions with limited persistence. Overall, the proposed framework provides a unified and interpretable approach for assessing complex pollutant–meteorology interactions across diverse locations and time.

**Keywords:** Pollutant-Weather Correlation, Shannon Entropy, Mutual Information, Principal Component Analysis, Transfer Entropy, Multi-city Comparison

## 1 Introduction

Air pollution remains one of the most pressing environmental health risks worldwide [1], particularly in urban regions where population density, industrial activity, and vehicular emissions converge to produce complex pollutant mixtures.

Understanding how atmospheric conditions influence the formation, transport, and transformation of pollutants is key to characterize the underlying dynamics of air quality. Air pollution dynamics can be viewed as a classic example of an open, driven-dissipative system [2–6] where energy and

matter continuously flow through chemical, physical, and weather-related processes, giving rise to persistent fluctuations in concentration levels. These far-from-equilibrium dynamics generate complex spatiotemporal patterns [7–11], shaped by both natural and anthropogenic factors and often described in terms of probability distributions rather than deterministic trends. From a physics perspective, such systems challenge classical equilibrium models and call for tools from nonlinear dynamics [12], stochastic processes [13], and information theory [14].

Pollutants (such as  $\text{PM}_{2.5}$ ,  $\text{PM}_{10}$ ,  $\text{SO}_2$  and  $\text{NO}_2$  and many more) are not merely passive tracers; they undergo nonlinear transformations [15], interact through feedback mechanisms [16], and are transported via advection-diffusion processes [17], all modulated by meteorological (such as temperature, precipitation etc.) forcing that introduce stochastic fluctuations. Understanding the interdependence between pollutants and weather variables is essential not only for accurate predictive modeling, environmental monitoring and air quality risk assessment, but also for uncovering emergent behavior in complex environmental systems [18, 19].

A substantial body of literature [20–22] has examined the relationships between air pollutant concentrations and meteorological variables. However, these investigations [23–25] have been overwhelmingly dominated by the use of a *single dependence measure*, most commonly linear correlation metrics, and are therefore limited in their ability to capture the complex and potentially nonlinear interactions that govern pollutant–meteorology dynamics. Moreover, these approaches overlook both non-stationarity [26] and directional causality. To address these limitations, we adopt an entropy based information-theoretic approach to study the interdependence of pollutants and weather variables. Although a small number of studies have employed nonlinear dependence measures, including mutual information [27], these measures are typically applied in isolation and are not combined with linear metrics within a unified analytical framework. In parallel, multivariate techniques such as principal component analysis (PCA) and clustering have largely focused on pollutant concentrations or meteorological variables independently [28, 29]. However,

the lack of a comprehensive measure integrating multiple forms of statistical dependence has constrained robust and comparable assessment of pollutant–meteorology interactions.

In this work, we address this issue by adopting an entropy-based information-theoretic framework, rooted in statistical physics and complex systems science, which provides powerful tools to characterize structure and dynamics in multivariate systems with inherent fluctuations [14, 30]. Metrics such as Shannon entropy [31], Mutual Information (MI) [32, 33], and Transfer Entropy (TE) [34] have proven valuable across fields from neuroscience to climate science [35, 36], and here we extend their application to urban air quality dynamics.

Using a multi-year dataset covering multiple Indian cities, we analyze interactions between the primary pollutants ( $\text{PM}_{2.5}$ ,  $\text{PM}_{10}$ ,  $\text{NO}_2$ , and  $\text{SO}_2$ ) and two of the most important meteorological variables (relative humidity RH and ambient temperature AT). We compute the Pearson correlation coefficient to estimate the linear correlations and use entropy-based measures to quantify uncertainty, dependency, and the directional flow of information [37, 38], thereby capturing both linear and non linear relationships.

The resulting correlation data across cities and variable pairs form a high-dimensional dataset that is complex to interpret directly due to the volume of observations and the multiple metrics involved. To systematically extract dominant patterns and reduce dimensional complexity, we amalgamate these diverse metrics into a unified measure of correlation. This is accomplished by employing Principal Component Analysis (PCA) [39, 40] to the set of correlation measures, enabling a consistent and comparable representation of pollutant–meteorology relationships across cities. PCA allows us to construct composite indices that summarize the overall strength and structure of pollutant–weather interactions, both within and across cities, by combining information from all three correlation metrics. To the best of our knowledge, this work presents the first implementation of a PCA-based compound indexing methodology for merging multi-metric correlation data between air pollutants and meteorological variables across spatial and variable dimensions.

Our results reveal spatial heterogeneity as well as similarities in pollutant–meteorological

couplings, suggesting that regional climate and geography play a fundamental role in shaping these dynamics. We find cities cluster into distinct groups with varying levels of interdependence. Additionally, the transfer entropy (TE) analysis provides clear evidence of bidirectional information flow across most cities. In particular, relative humidity (RH) generally exhibits a leading influence on the pollutants, whereas ambient temperature (AT) tends to display the opposite, lagging behavior, with respect to most pollutants. The time delayed mutual information (TDMI) analysis further reveals that, for the majority of cities, the dependence between particulate matter (PM<sub>2.5</sub> and PM<sub>10</sub>) and RH peaks at zero lag and decays approximately exponentially with increasing lag. This behavior reflects a short memory and limited temporal persistence in the underlying stochastic dynamics. Only in a subset of cities, similar trend is also observed for the gaseous pollutants (NO<sub>2</sub> and SO<sub>2</sub>) with RH.

The sequential key steps of our multi-stage analysis are summarized in the following technical roadmap, providing a structured overview that guides the detailed methodology in the subsequent sections:

- **Data preparation and preliminary analysis:** The first stage consists of compilation and pre-processing of multi-city pollutant and meteorological time series, including missing-value treatment. We also investigate the temporal trends and nonlinear pollutant–weather interactions at this stage.
- **Static dependency estimation:** At the next stage, mutual correlation among each pollutant–meteorology pair is estimated using three different static measures, namely, Pearson correlation, mutual information, and relative conditional entropy.
- **Intra-city integration:** A Local Correlation Strength for each city is estimated by combining the multiple dependency measures using principal component analysis for all variable pairs.
- **Cross-city aggregation (Composite Score  $C$ ):** The spatial variability of the pollutant–weather correlation is investigated at two levels. A Spatial Correlation Score (SCS) is computed using PCA for each variable pair across all the cities. Finally, once again we use PCA

to determine a comprehensive correlation score (CCS) combining the SCS across all the variable pairs and all cities. The overall pollutant–meteorology coupling strength  $C$  enables the classification of cities into distinct interaction regimes.

- **Temporal dependency analysis:** The mutual temporal dependency of pollutant–weather variable pairs is estimated using transfer entropy (TE) and time-delayed mutual information (TDMI). This analysis is used to characterize causal directionality, lag effects, and persistence in pollutant–weather interactions.

The remainder of the paper is organized as follows: Sec. 2 describes the datasets and methods used in this study, including preliminary analyses of temporal trends. Sec. 3 presents the results of correlation analyses, PCA-based compound indexing, and temporal dependency assessments. Sec. 4 interprets these results, highlighting their implications and limitations. Finally, Sec. 5 provides concluding remarks and discusses potential future directions.

## 2 Data and Methods

This section describes the datasets and methods used in the study.

### 2.1 Study Location, Sources and Collection Period

The data used in this study is obtained from the Central Pollution Control Board (CPCB) of India [41], which provides publicly available, quality-assured environmental monitoring data. The dataset comprises daily average concentrations of various atmospheric pollutants and meteorological variables collected from various monitoring stations ( $N_m$ ), which recorded the required set of variables in each location across multiple cities [see Table 8 in Appendix for a summary]. To be precise, data is collected from 87 monitoring stations, across 24 cities [42], including seven Tier-1 cities (characterized by high population density, robust infrastructure and economic activity) and seventeen Tier-2/3 cities (smaller urban centers with growing population and developing infrastructure). The selected cities

represent the geographic, climatic, demographic, and industrial diversity of India, encompassing a range of population densities, emission sources, and meteorological conditions [43–45]. The choice is also based on the availability of continuous, high-quality air pollution and meteorological data. While not exhaustive, the 87 monitoring stations across these cities provide sufficient coverage to capture representative national-scale air quality dynamics and allow a comprehensive comparative study of pollutant–meteorology interactions.

**Selected Environmental Parameters:** In our analysis, we focus on a set of key variables representing both air pollutants and meteorological factors. Specifically, we select  $\text{PM}_{2.5}$  (particulate matter with diameter  $< 2.5 \mu\text{m}$ ),  $\text{PM}_{10}$  (particulate matter with diameter  $< 10 \mu\text{m}$ ),  $\text{NO}_2$  (nitrogen dioxide) and  $\text{SO}_2$  (sulfur dioxide) due to their known impact on air quality and human health [1]. Among these,  $\text{PM}_{2.5}$  and  $\text{PM}_{10}$  are categorized as particulate (matter-type) pollutants, while  $\text{NO}_2$  and  $\text{SO}_2$  are gaseous pollutants. In addition two meteorological parameters— RH (relative humidity, expressed as a percentage, representing the amount of moisture in the air relative to the maximum it can hold at a given temperature) and AT (ambient temperature, measured in degrees Celsius, indicating the surrounding air temperature) are included, given their influence [46, 47] on pollutant dispersion and chemical transformation in the atmosphere. Relative humidity (RH) affects aerosol hygroscopic growth, altering particle size, light scattering, and deposition rates, and thereby directly modulating  $\text{PM}_{2.5}$  concentrations. Ambient temperature (AT) controls atmospheric stability, influencing both the dilution of pollutants and the rates of secondary aerosol formation. Together, RH and AT capture key thermodynamic and dynamical processes that jointly govern short-term variability in particulate matter.

The choice of these variables is guided by both data availability and their relevance to the study objectives.

## 2.2 Data Pre-processing

Environmental data often suffer from missing values and sensor noise due to hardware failures, power outages, or maintenance activities. To address this issue and to smooth the time

series for reliable analysis, we employ Kalman filtering [48, 49], a recursive optimal estimation technique widely used for noisy time series data. For the datasets used in this study, the average proportion of missing observations is relatively low, amounting to approximately 2.15% for  $\text{PM}_{2.5}$ , 3.27% for  $\text{PM}_{10}$ , 2.41% for  $\text{SO}_2$ , and 2.47% for  $\text{NO}_2$ . Meteorological variables exhibit slightly higher missing rates, with relative humidity (RH) and Ambient Temperature (AT) having approximately 4.08% and 5.23% missing values, respectively. We apply the Kalman filter [50] separately to each time series (for all the pollutants and meteorological parameters) for each city. The filter not only interpolates missing values but also de-noises the observed signals, preserving the underlying dynamics critical for entropy and information-theoretic analyses.

The effectiveness of missing value imputation using Kalman Filtering is evaluated across all monitoring stations in 24 cities. To this end, a sensitivity analysis is conducted by artificially removing a subset of observed data and reconstructing them using the Kalman filter for four air pollutants ( $\text{PM}_{2.5}$ ,  $\text{PM}_{10}$ ,  $\text{NO}_2$ , and  $\text{SO}_2$ ) and two meteorological variables (AT and RH). The imputation accuracy is quantified using the root mean square error (RMSE) [51] between the observed and reconstructed values. Consistently low and stable RMSE values across all cities and variables confirm that Kalman filtering is an effective and robust method for handling missing observations in our study.

## 2.3 Preliminary Analysis

This study employs a multi-layered, entropy-based approach to investigate the interdependence and directional relationships between air pollutants and meteorological variables in Indian cities. As a starting point, a preliminary analysis is conducted to explore the complex temporal behavior of key pollutants and meteorological parameters. This includes generating time series plots and applying non-parametric regression techniques to identify underlying trends and patterns across different regions. To provide a baseline understanding and quantitative overview of the data, we present the mean ( $\langle \rho \rangle$ ) and standard deviation ( $\sigma$ ) of all pollutants and meteorological variables considered

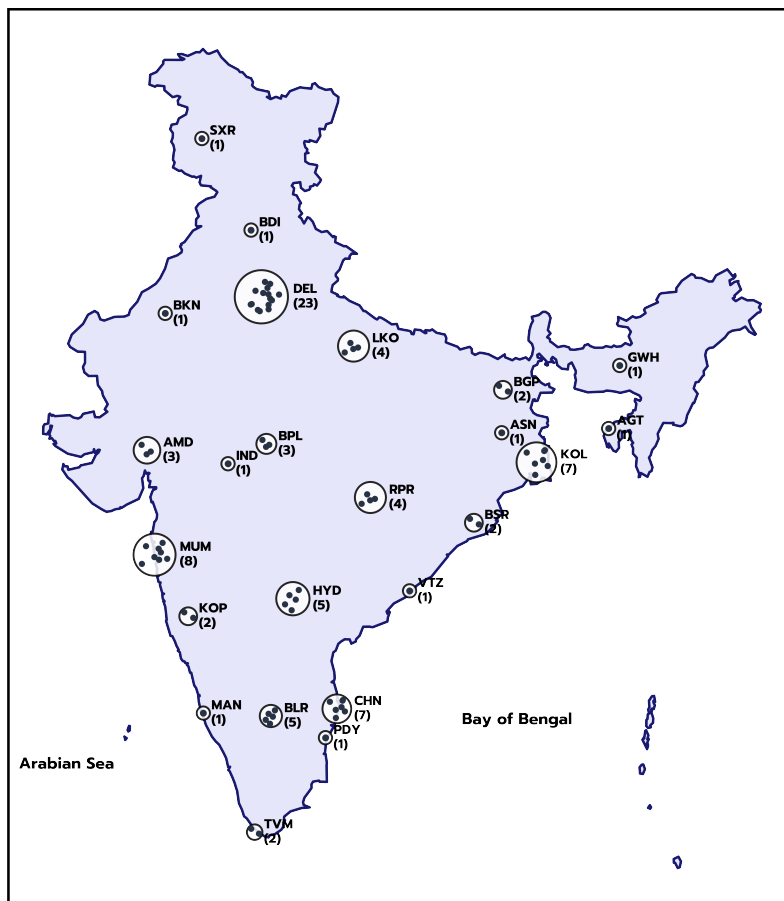


**Fig. 1** Map of India depicting monitoring stations across the studied cities. Individual stations are shown as dots, and the total number of stations is indicated for each city.

in this study obtained by averaging them across stations in Table 9 (see Appendix).

### 2.3.1 Temporal Trends

To visually examine temporal fluctuations and possible seasonal patterns, time series plots of the pollutant concentrations and meteorological variables are generated for each location. Fig. 2 depicts such time series plots for two representative stations, namely, Jadavpur in Kolkata and Sion in Mumbai.

Each panel stacks five years of daily data for six variables -  $PM_{2.5}$ ,  $PM_{10}$ ,  $SO_2$ ,  $NO_2$ , RH and AT, so that seasonal patterns amid stochastic fluctuations can be compared at a glance. Both  $PM_{2.5}$  and  $PM_{10}$  surge each winter reaching their peaks around Dec-Jan, and decrease during the warm, humid monsoon months pointing to strong seasonality and common sources. Both the weather

variables RH and AT show an almost reverse trend, they reach their minimum during Dec-Jan and become maximum in the summer and monsoon months.  $SO_2$  remains near background levels ( $< 10 \mu g m^{-3}$ ) except for a few short spikes, while  $NO_2$  is likewise low save for few dramatic spikes above 100, reflecting intermittent fluctuations probably driven by local events. From these plots for each city, a clear trend emerges:  $PM_{2.5}$  and  $PM_{10}$  levels show a strong positive correlation, indicating that they tend to rise and fall together. In contrast,  $PM_{2.5}$  levels (also the other pollutants) appear to be inversely related to relative humidity (RH), suggesting an anti-correlation where higher humidity is generally associated with lower  $PM_{2.5}$  concentrations.

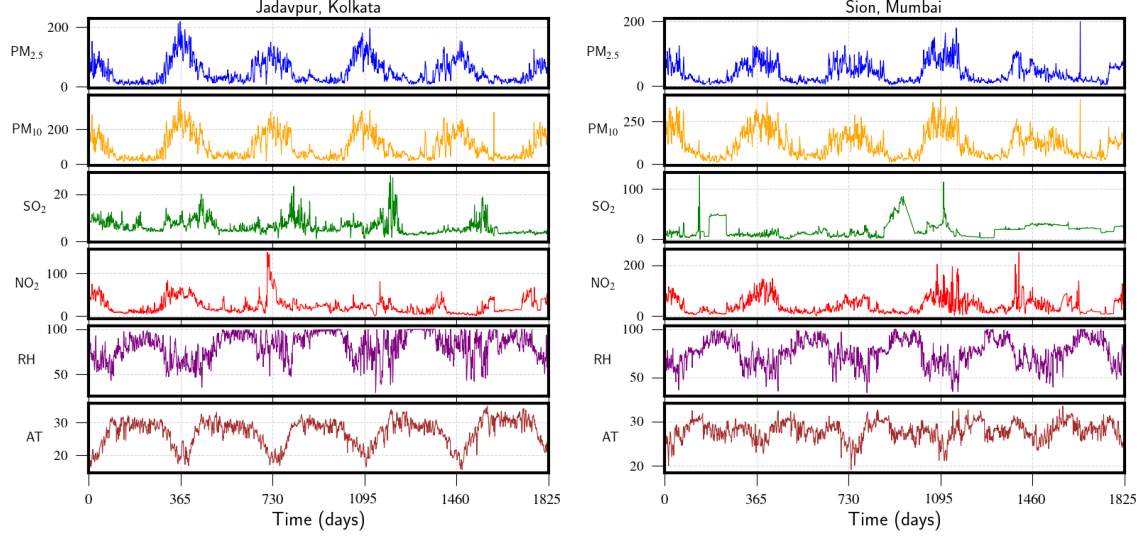


**Fig. 2** Time-series plots for concentration of the pollutants and the meteorological parameters for two representative stations in Kolkata (left panel) and Mumbai (right panel) for the period Jan, 2020 to Dec, 2024.

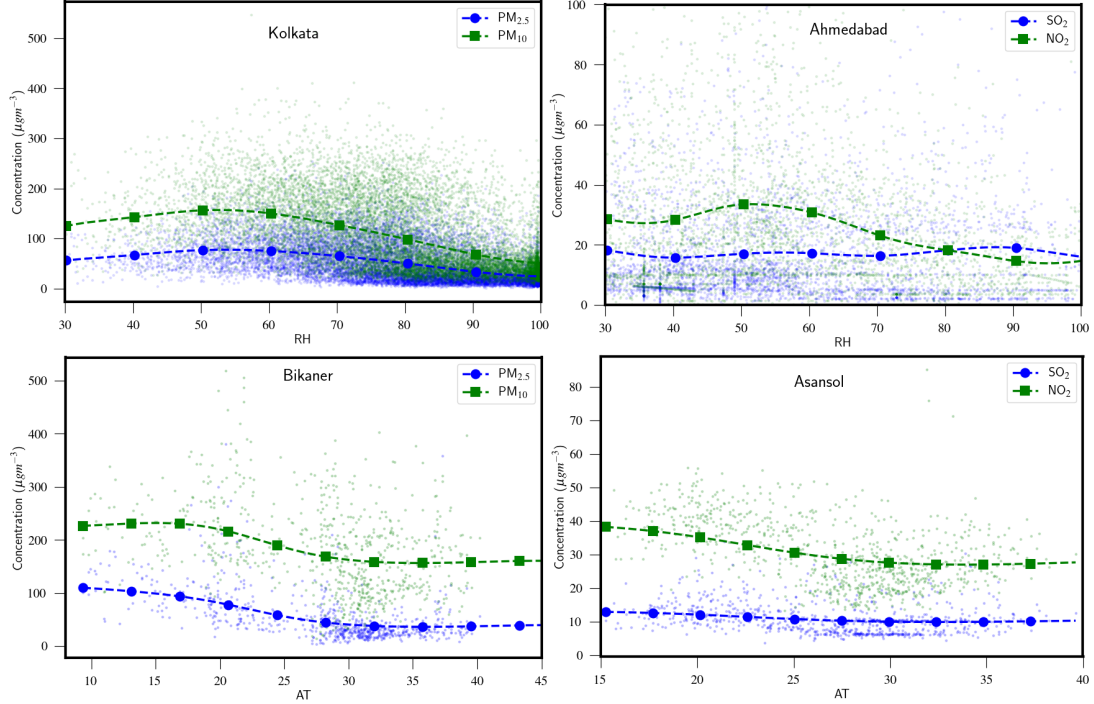


**Fig. 3** Kernel regression plots illustrating relationships between pollutants and meteorological variables in selected cities.

### 2.3.2 Nonlinearity in Correlation

To complement the time-series diagnostics, we next explore the instantaneous relationships between each air-quality indicator (PM<sub>2.5</sub>, PM<sub>10</sub>,

NO<sub>2</sub>, SO<sub>2</sub>) and the two meteorological drivers (RH, AT). For every pollutant–weather variable pair we pool the full five-year daily dataset and fit a non-parametric regression smoothing with a

kernel regression framework [52]. In statistics, kernel regression is a non-parametric method used to detect the type of relationship present between random variables  $X$  and  $Y$ . The regression takes the form,

$$E(Y|X) = m(X) \quad (1)$$

where  $E(Y|X)$  denotes the expectation value of  $Y$ , conditioned on  $X$ , and  $m$  is an unknown function. A common estimator for this function is the Nadaraya–Watson estimator,

$$\hat{m}(x) = \frac{\sum_{i=1}^N K_h(x - X_i) Y_i}{\sum_{i=1}^N K_h(x - X_i)}, \quad (2)$$

with  $Y_i$  as the pollutant concentration,  $X_i$  the weather variable, and  $K_h(z)$  is a Gaussian kernel with bandwidth  $h$  selected via leave-one-out cross-validation [53, 54]. This approach places more weight on observations whose meteorological conditions are close to the point of interest, without imposing a parametric shape, thereby naturally handling fluctuations across scales.

Figure 3 show the kernel regression plots for different pairs of pollutant-meteorological parameters for a few representative cities.

These plots demonstrate clear nonlinear relationships between the pollutants and meteorological variables, indicating that traditional linear methods may not adequately assess the complexity of these interactions.

## 2.4 Correlation Analysis of Pollutants and Weather variables

In light of the nonlinear relationships identified in the preliminary analysis, the subsequent analysis focuses on systematically characterizing the associations among air pollutants and meteorological parameters. To ensure a robust and comprehensive characterization of these relationships, we employ a multi metric approach that accounts for diverse interaction patterns. We focus on three complementary correlation metrics: Pearson coefficient, mutual information, and relative conditional entropy. While the Pearson coefficient estimates the linear dependencies, the other two entropy based measures are more general, and are able to characterize non-linear and asymmetric dependencies, as well as variability arising from fluctuations across timescales.

We now discuss the methods used to compute each of the three metrics in details to understand their individual pollutant-weather relationships and lay the groundwork for the construction of a unified metric in a later section.

### 2.4.1 Pearson Correlation Coefficient

The simplest quantitative estimate of the linear interdependency of two observables is the Pearson correlation coefficient (PCC) [55]. The PCC between two time series  $X = \{x_1, x_2, \dots, x_N\}$  and  $Y = \{y_1, y_2, \dots, y_N\}$  is defined as,

$$r_{X,Y} = \frac{\sum_{t=1}^N (x_t - \hat{x})(y_t - \hat{y})}{\sqrt{\sum_{t=1}^N (x_t - \hat{x})^2} \sqrt{\sum_{t=1}^N (y_t - \hat{y})^2}}, \quad (3)$$

where,  $\hat{x} = \frac{1}{N} \sum_{t=1}^N x_t$  and  $\hat{y} = \frac{1}{N} \sum_{t=1}^N y_t$  are the means of the respective time-series. Here  $N$  denotes the length of the time-series, which, for our case varies from station to station. Clearly, PCC is symmetric under the exchange of  $X$  and  $Y$  and its values are bounded by  $-1 \leq r_{X,Y} \leq 1$ . While a perfect positive (negative) linear correlation between  $X$  and  $Y$  is indicated by  $r_{X,Y} = 1$  ( $r_{X,Y} = -1$ ),  $r_{X,Y} = 0$  indicates absence of linear correlation.

For each of the selected cities, we compute the PCC between the eight pollutant-weather variable pairs, namely,  $\text{PM}_{2.5}\text{-RH}$ ,  $\text{PM}_{2.5}\text{-AT}$ ,  $\text{PM}_{10}\text{-RH}$  etc. To this end, we first compute the PCC value  $r_{X,Y}^k$  between the pollutant  $X$  and weather variable  $Y$  from the corresponding time-series data from the  $k$ -th station. The PCC  $r_{X,Y}$  for the entire city is then obtained by averaging over all the stations in the city,

$$r_{X,Y} = \frac{1}{N_m} \sum_{k=1}^{N_m} r_{X,Y}^k, \quad (4)$$

where  $N_m$  denotes the total number of monitoring stations in a city.

### 2.4.2 Mutual Information

To further explore the dependence structure between air pollutants and weather variables, we compute the mutual information [33, 56]. MI quantifies the reduction in uncertainty of one variable given knowledge of the other, characterizing both linear and non-linear dependencies. The

mutual information between air pollutants ( $X$ ) and meteorological factors ( $Y$ ) is defined as

$$I_{X,Y} = S_X + S_Y - S_{X,Y}, \quad (5)$$

where  $S_X$  and  $S_Y$  represent the self-entropy (Shannon Entropy) of variables  $X$  and  $Y$ , respectively, and  $S_{X,Y}$  denotes their joint entropy.

Let  $p(x)$  denote the probability density function (PDF) of the stationary time-series  $X = \{x_t; t = 1, \dots, N\}$ . The corresponding Shannon entropy, which quantifies the average uncertainty or information content in a PDF, is defined as,

$$S_X = - \int dx p(x) \ln[p(x)]. \quad (6)$$

Higher entropy values indicate greater uncertainty or disorder in the system. The joint entropy  $S_{X,Y}$ , which quantifies the combined uncertainty of both variables, is defined as,

$$S_{X,Y} = - \int dx \int dy p(x,y) \ln[p(x,y)], \quad (7)$$

where  $p(x,y)$  denotes the joint probability density of  $X$  and  $Y$ .

We construct the probability distribution function (PDF) of each observable (all pollutants and weather variables) from the aggregated data from all the stations in each city. The joint distributions of each pollutant-weather variable pair is also constructed from the same data. The self-entropies of each observable and the mutual information of the pollutant-weather variables pairs are computed from these distributions.

### 2.4.3 Relative Conditional Entropy

To further estimate the strength, complexity and conditional structure of interactions between air pollutants ( $X$ ) and meteorological factors ( $Y$ ), (both linear and non-linear), we compute relative conditional entropy. The conditional entropy for a pollutant ( $X$ ), given a weather variable ( $Y$ ) is defined as,

$$\mathcal{H}_{X;Y} = S_{X,Y} - S_Y, \quad (8)$$

where  $S_{X,Y}$  and  $S_Y$  denote the joint entropy of  $X$  and  $Y$  [see Eq. (7)] and self-entropy of  $Y$  [see Eq. (6)], respectively. We compute the self

entropy of each pollutant ( $X$ ) and weather variable ( $Y$ ) across all cities and reported these values in Table 10 in Appendix. To characterize the fraction of uncertainty remaining in  $X$  after conditioning on  $Y$ , it is useful to define a relative conditional entropy as,

$$\mathcal{H}_{X;Y}^R = \mathcal{H}_{X;Y} / S_X. \quad (9)$$

It can be easily shown that  $0 \leq \mathcal{H}_{X;Y}^R \leq 1$ . Smaller values of  $\mathcal{H}_{X;Y}^R$  indicate that  $X$  has a strong dependence on  $Y$ , while  $\mathcal{H}_{X;Y}^R = 1$  indicates complete independence of the two variables.

## 2.5 PCA-based Compound Scoring Framework for Pollutant–Meteorological Correlation Strength

The different metrics discussed so far, namely, Pearson correlation, relative conditional entropy and MI, complement each other in characterizing the interdependence of the pollutants and weather variables. While individual correlation measures can highlight pairwise relationships between pollutants and meteorological variables, a more comprehensive understanding requires integrating these metrics and scaling the analysis across different spatial levels. To develop a unified measure of the correlations, we employ Principal Component Analysis (PCA) [39, 40], a well established technique frequently used in the development of composite indices. PCA provides a rigorous statistical framework for identifying latent structures in multivariate data by projecting it onto orthogonal axes (principal components) that maximize variance. In the context of correlation analysis, PCA allows us to construct composite indices that summarize the overall strength and structure of pollutant–weather interactions, both within and across cities, by combining information from all three correlation metrics. This dimensionality reduction in multivariate datasets facilitates the development of interpretable and scalable indices that can be used to compare locations, identify regional trends, and support further modeling.

To describe PCA from a general perspective, let us consider a dataset with  $p$  features, each measured over  $m$  observations. For our case, a feature can be a specific correlation measure or a

pollutant-weather variable pair, while an observation can be a particular pollutant-weather pair or a city, depending on the context. The data can be represented as a matrix of dimension  $m \times p$  where each row corresponds to an observation and each column to a feature. The element  $x_{jk}$  denotes the value of feature  $k$  for observation  $j$ . Prior to applying PCA, the data are standardized to ensure all features are on a comparable scale. Each element is transformed to its Z-score form,

$$z_{jk} = \frac{x_{jk} - \mu_k}{\sigma_k},$$

$$\forall j = 1, 2, \dots, m \text{ and } k = 1, 2, \dots, p, \quad (10)$$

where  $\mu_k = \frac{1}{m} \sum_{j=1}^m x_{jk}$  denotes the mean of  $k$ -th feature over the  $m$  observations and  $\sigma_k$  denotes the corresponding standard deviation.

This step ensures that all metrics are placed on a common scale, allowing for meaningful combination despite differences in their original units and distributional characteristics. PCA is then performed on the resulting standardized matrix, yielding a set of principal components ordered by the amount of variance they contain. In each case, we retain only the first principal component (PC1), which contains the largest share of total variance, and is given by,

$$\text{PC1}_j = \sum_{k=1}^p w_k \cdot z_{jk}, \quad (11)$$

where  $w_k$  is the loading (i.e., the weight) of the  $k$ -th feature. The first principal component accounts for the maximum amount of variability of the features compared to all the other principal components formed after the dimensional reduction. Thus,  $\text{PC1}_j$  can be interpreted as a unified measure for all the features for the  $j$ -th observation.

To systematically interpret the complex inter-dependencies between air pollutants and meteorological variables across multiple locations, through a unified measure of correlation strength, we employ a three-tiered PCA-based correlation aggregation framework.

- At the first level, intra-city correlation strengths are computed for each pollutant-weather variable pair, capturing localized interactions

within individual cities. In this case, ‘observation’ refers to the eight different pollutant-weather variable pairs, i.e.,  $m = 8$  while ‘feature’ refers to the different measures of correlation, i.e.,  $p = 3$ .

- The second level involves inter-city aggregation, wherein correlation strengths for each variable pair are consolidated across cities to reveal broader spatial patterns. In this case, each ‘observation’ corresponds to a city ( $m = 24$ ) whereas each ‘feature’ represents a distinct correlation metric ( $p = 3$ ).
- Finally, these pairwise insights are combined into a comprehensive correlation score (CCS) that encapsulates the overall degree of correlation between pollution and weather correlations across the network. Here the ‘observation’ refers to the 24 cities ( $m = 24$ ) and the ‘features’ correspond to the different pollutant-weather variable pairs ( $p = 8$ ).

**Sensitivity Analysis:** To investigate the influence of different pairs of pollutant-weather correlations to the values of CCS across multiple cities, we conduct a PCA-based sensitivity analysis [57–59]. This analysis quantifies how the exclusion of each individual pollutant-weather pair affects the overall comprehensive correlation score, allowing us to assess the relative contribution of each interaction to the city-level correlation structure.

## 2.6 Temporal Correlation

It is important to go beyond static correlation measures and investigate the temporal dynamics between pollutants and meteorological variables to uncover potential causal linkages and directional dependencies. In this subsection the variable pairs are subjected to time-domain analysis using two complementary techniques, namely Transfer Entropy (TE) and time-delayed Mutual Information (TDMI). This approach allows us to explore both the directionality and temporal structure of interactions, providing insights into the lead-lag behavior and potential causal links underlying pollutant-weather dynamics.

### 2.6.1 Causal Interaction: Transfer Entropy

We utilize transfer entropy [34, 60], a non-parametric information-theoretic measure to

explore the directional dependencies and potential causal interactions between air pollutants and meteorological parameters. TE quantifies the amount of information that past values of a meteorological variable convey about the future evolution of a pollutant (and vice versa) beyond what is already contained in each series' own history and thereby indicates possible causal influence. TE from a process  $Y$  to another process  $X$  is defined as,

$$\mathcal{T}_{Y \rightarrow X} = \mathcal{H}_{X_t; X_{t-1}} - \mathcal{H}_{X_t; X_{t-1}, Y_{t-1}}, \quad (12)$$

where  $\mathcal{H}_{X_t; X_{t-1}}$  is the conditional entropy of  $X_t$ , given its recent past value  $X_{t-1}$  [see Eq. (8)]. Moreover,  $\mathcal{H}_{X_t; X_{t-1}, Y_{t-1}}$  denotes entropy of  $X_t$ , conditioned on the past values of both  $X$  and  $Y$ , given by,

$$\mathcal{H}_{X_t; X_{t-1}, Y_{t-1}} = S_{X_t, X_{t-1}, Y_{t-1}} - S_{X_{t-1}, Y_{t-1}}, \quad (13)$$

where  $S_{X_{t-1}, Y_{t-1}} = S_{X, Y}$  is the joint entropy of  $X$  and  $Y$ , defined in Eq. (7), and

$$S_{X_t, X_{t-1}, Y_{t-1}} = - \int dx_t \int dx_{t-1} \int dy_{t-1} \\ \times p(x_t, x_{t-1}, y_{t-1}) \ln p(x_t, x_{t-1}, y_{t-1}), \quad (14)$$

denotes the joint entropy of  $X$  with past values of itself and  $Y$ . Using Eqs. (13)-(14), Eq. (12) simplifies to,

$$\mathcal{T}_{Y \rightarrow X} = S_{X_t, X_{t-1}} - S_{X_t, X_{t-1}, Y_{t-1}} + S_{X, Y} - S_X, \quad (15)$$

Note that,  $\mathcal{T}_{Y \rightarrow X}$  is not symmetric in  $X$  and  $Y$ . A positive  $\mathcal{T}_{Y \rightarrow X}$  implies that past values of  $Y$  has a directional effect on present values of  $X$ . This helps in identifying causal relationships, such as whether changes in  $Y$  precede changes in  $X$  or vice versa.

### 2.6.2 Time-Delayed Mutual Information

To further explore the temporal dependence between pollutant and weather variables, we compute the mutual information with a time delay,  $\tau$ , considering pollutant at day  $t$  and meteorological parameter at a later day  $t + \tau$ . For two stationary time-series  $X = \{x_t\}_{t=1}^N$  (pollutant)

and  $Y = \{y_t\}_{t=1}^N$  (weather variable), TDMI for a given lag  $\tau$  is defined as,

$$I_{X, Y}(\tau) = \sum_{x_t} \sum_{y_{t+\tau}} p(x_t, y_{t+\tau}) \ln \left[ \frac{p(x_t, y_{t+\tau})}{p(x_t)p(y_{t+\tau})} \right], \quad (16)$$

where  $p(x_t, y_{t+\tau})$  is the joint probability distribution of  $(X_t, Y_{t+\tau})$  and  $p(x)$ ,  $p(y)$  are the corresponding marginals. Equivalently, in terms of entropies, we can write,

$$I_{X, Y}(\tau) = S_X + S_Y - S_{X_t, Y_{t+\tau}}, \quad (17)$$

with  $S_{X_t, Y_{t+\tau}}$  denoting the joint entropy. TDMI thus quantifies lagged statistical dependencies between pollutant and weather variables.

## 3 Results

In this section, we present the main findings of our study, focusing on static and dynamic inter-dependencies of air pollutants and meteorological variables across the study regions. The results are organized into three main subsections. First, we analyze the static inter-dependencies among the variables. Next, we compute the correlation score depending on PCA based framework for intra-city as well as inter-city aggregation. Finally, we explore the temporal dynamics of the variables to understand the directional dependencies between variable pairs.

### 3.1 Static Dependency Analysis

This subsection examines the static relationships between air pollutants and meteorological variables. The main findings for three complementary measures employed to quantify these associations are discussed below.

#### 3.1.1 Pearson Correlation

The PCC values computed from Eqs. (3) and (4) for the twenty four selected cities are summarized in Table 1. It appears that  $r_{\text{PM}_{2.5}, \text{RH}} < 0$  for most of the cities, which indicates that  $\text{PM}_{2.5}$  and relative humidity affect each other negatively, at least to linear order. A similar trend is observed for  $\text{PM}_{10}$ , with RH showing a negative correlation with it in most locations, reinforcing the

City	$r_{PM_{2.5},RH}$	$r_{PM_{2.5},AT}$	$r_{PM_{10},RH}$	$r_{PM_{10},AT}$	$r_{SO_2,RH}$	$r_{SO_2,AT}$	$r_{NO_2,RH}$	$r_{NO_2,AT}$
AMD	-0.278	-0.163	-0.305	-0.151	-0.151	-0.020	-0.012	-0.027
BLR	-0.191	0.038	-0.312	0.116	-0.188	-0.047	0.044	0.016
CHN	0.044	-0.290	-0.084	-0.222	-0.025	-0.139	0.051	-0.182
DEL	0.189	-0.562	-0.085	-0.407	-0.062	-0.338	-0.331	-0.005
HYD	-0.394	-0.171	-0.497	-0.060	-0.283	-0.093	0.137	0.173
KOL	-0.425	-0.522	-0.476	-0.503	-0.283	-0.283	-0.415	-0.172
MUM	-0.544	-0.214	-0.561	-0.170	-0.473	-0.182	0.023	-0.001
AGT	0.098	-0.239	-0.019	-0.284	0.033	-0.154	-0.158	-0.297
ASN	-0.353	-0.491	-0.385	-0.534	-0.431	-0.486	-0.507	-0.280
BDI	0.088	-0.578	-0.128	-0.373	0.102	-0.621	-0.036	-0.410
BGP	-0.032	-0.633	-0.238	-0.381	-0.238	-0.275	0.137	0.047
BPL	-0.188	-0.536	-0.393	-0.373	-0.509	-0.350	-0.226	-0.009
BSR	-0.295	-0.661	-0.340	-0.568	-0.214	-0.758	-0.302	-0.145
BKN	0.009	-0.544	-0.408	-0.357	-0.317	-0.348	-0.270	-0.338
GWH	-0.077	-0.482	-0.122	-0.422	0.018	-0.300	0.312	0.117
IND	-0.197	-0.304	-0.505	-0.106	-0.537	-0.176	-0.485	0.128
KOP	-0.487	0.017	-0.618	0.067	-0.609	0.054	-0.416	0.070
LKO	-0.093	-0.376	-0.331	-0.272	-0.188	-0.165	-0.101	0.035
MAN	0.085	0.001	0.135	-0.013	-0.468	0.303	-0.366	-0.090
PDY	-0.023	-0.303	-0.297	-0.095	-0.011	-0.439	-0.247	0.248
RPR	-0.381	-0.294	-0.435	-0.254	-0.545	-0.125	-0.422	0.293
SXR	-0.100	0.007	-0.018	-0.067	-0.028	-0.246	-0.086	-0.096
TVM	-0.327	0.120	-0.366	0.211	0.006	0.079	0.009	0.128
VTZ	-0.175	-0.434	-0.157	-0.205	-0.151	-0.101	0.158	-0.032

**Table 1** Pearson Correlation Coefficients of pollutants and weather variables across cities with maximum 7% margin of error. Blue colored cells highlight positive correlation.

idea that moisture in the air can suppress particulate matter levels. Ambient temperature (AT), too, tends to correlate negatively with  $PM_{2.5}$  and  $PM_{10}$  across many cities, especially in urban centers like Kolkata, Delhi, Mumbai and Asansol, where cooler temperatures may coincide with poor dispersion conditions or increased local emissions, leading to pollutant accumulation. For gaseous pollutants like  $SO_2$  and  $NO_2$ , the relationships are more varied. While several cities show weak or inconsistent correlations, others (e.g., Kolkata, Asansol, Bhubaneswar, and Bikaner) display significant negative correlations. Overall, both RH and AT have a measurable influence on air pollutant concentrations, particularly for particulate matter, and that these meteorological variables should be considered when analyzing or forecasting urban air quality.

### 3.1.2 Mutual Information

Mutual Information ( $I_{X,Y}$ ) values are computed using the self entropy [see Eq. (6)] and joint

entropy [see Eq. (7)] of the corresponding pollutant and meteorological variables. Table 10 (Appendix) summarizes the self-entropy values indicating their individual uncertainty levels. It is apparent from this table that across cities the uncertainty ranking is roughly  $S_{PM_{10}} \geq S_{PM_{2.5}} > S_{NO_2} \sim S_{RH} > S_{SO_2} > S_{AT}$ , highlighting that particulates fluctuate most from day to day, while temperature is comparatively stable.

The total amount of shared information between pollutant and meteorological variables is estimated by computing  $I_{X,Y}$  using Eq. (5), (6) and (7) for all variable pairs, across all cities. Table 2 summarizes MI between each pollutant and the two meteorological drivers (RH, AT) for all cities. Broadly, particulates show the strongest weather links, often tighter with humidity than temperature: e.g.  $I_{PM,RH}$  exceeds  $I_{PM,AT}$  in Ahmedabad, Bengaluru, Hyderabad, Mumbai, Kolhapur, etc., while a few places (Chennai, Kolkata) show comparable or higher  $I_{PM,AT}$ . Several cities stand out with consistently high  $I$  across many pairs notably Asansol (lying in the range 0.47 – 0.60

City	$I_{PM_{2.5},RH}$	$I_{PM_{2.5},AT}$	$I_{PM_{10},RH}$	$I_{PM_{10},AT}$	$I_{SO_2,RH}$	$I_{SO_2,AT}$	$I_{NO_2,RH}$	$I_{NO_2,AT}$
AMD	0.180	0.144	0.196	0.151	0.153	0.106	0.162	0.136
BLR	0.073	0.023	0.117	0.059	0.064	0.030	0.097	0.047
CHN	0.076	0.110	0.054	0.112	0.082	0.088	0.069	0.091
DEL	0.105	0.240	0.092	0.139	0.060	0.022	0.017	0.078
HYD	0.204	0.073	0.234	0.076	0.082	0.127	0.128	0.111
KOL	0.212	0.265	0.221	0.269	0.043	0.018	0.082	0.104
MUM	0.268	0.071	0.305	0.061	0.031	0.080	0.166	0.067
AGT	0.400	0.515	0.360	0.554	0.272	0.406	0.389	0.502
ASN	0.597	0.602	0.599	0.570	0.555	0.534	0.475	0.536
BDI	0.329	0.516	0.347	0.439	0.456	0.499	0.357	0.531
BGP	0.280	0.414	0.279	0.296	0.120	0.156	0.215	0.289
BPL	0.333	0.380	0.381	0.332	0.223	0.256	0.403	0.361
BSR	0.496	0.726	0.488	0.653	0.274	0.355	0.504	0.755
BKN	0.521	0.559	0.703	0.535	0.333	0.350	0.530	0.499
GWH	0.348	0.470	0.385	0.469	0.474	0.439	0.242	0.325
IND	0.244	0.241	0.451	0.304	0.254	0.159	0.406	0.308
KOP	0.471	0.196	0.617	0.310	0.240	0.086	0.553	0.246
LKO	0.145	0.198	0.180	0.160	0.203	0.184	0.118	0.103
MAN	0.311	0.230	0.339	0.293	0.512	0.599	0.297	0.309
PDY	0.208	0.229	0.301	0.245	0.260	0.208	0.208	0.306
RPR	0.253	0.163	0.301	0.220	0.184	0.195	0.317	0.206
SXR	0.222	0.272	0.247	0.298	0.176	0.293	0.312	0.450
TVM	0.183	0.253	0.144	0.253	0.263	0.416	0.110	0.158
VTZ	0.196	0.292	0.209	0.267	0.162	0.166	0.162	0.216

**Table 2** Mutual Information values for the eight pollutant-meteorological variable pairs across the selected cities. For each pair, the maximum and minimum MI values are highlighted in blue and red, respectively.

for most pairs), Agartala, Baddi, Bhubaneswar, Bikaner, and Kolhapur for  $I_{PM_{10},RH}$  (0.617). The largest value of  $I$  in the table is  $I_{NO_2,AT}$  in Bhubaneswar (0.755), indicating strong temperature control on  $NO_2$  there;  $I_{PM_{10},RH}$  in Bikaner (0.703) and PM pairs in Asansol (0.60) are also prominent. For  $SO_2$ , the strongest dependencies tend to be with AT in certain climates e.g., Mangaluru (0.599), Thiruvananthapuram (0.416), Srinagar (0.293) suggesting thermally driven chemistry or sources, whereas other cities show modest  $SO_2$ -weather coupling. Coastal metros like Mumbai display higher  $I_{PM,RH}$  (0.268 – 0.305) but weaker  $I_{PM,AT}$ , consistent with moist boundary-layer effects. Overall,  $I$  values are city-specific, but the common pattern is  $I_{PM \leftrightarrow RH} > I_{PM \leftrightarrow AT}$ , while  $NO_2$  often tracks AT, and  $SO_2$  shows mixed but sometimes temperature-led behavior.

### 3.1.3 Relative Conditional Entropy

The values of the conditional entropy,  $\mathcal{H}$ , i.e., the uncertainty left in each pollutant after conditioning on RH or AT, computed from the aggregated

data across all the chosen cities using Eq. (8) are tabulated in Table 11 [see in Appendix]. The relative conditional entropy  $\mathcal{H}^R$  (i.e, fraction of uncertainty remaining) in Table 3 is also calculated using the aggregated data from all selected cities using Eq. (9). High  $\mathcal{H}^R$  values close to 1 (shown in blue) indicate that meteorological factors explain very little of the pollutant variability. In contrast, low  $\mathcal{H}^R$  values (shown in red) suggest that RH and AT account for a significant portion of the variability in pollutant levels. In summary, smaller  $\mathcal{H}^R$  values imply that meteorological parameters are highly informative about pollutant concentrations, whereas higher or near-unity values indicate that pollutant variations are largely independent of RH and AT.

The three metrics discussed in this section capture various aspects of the pollutant-weather interactions. A consolidated summary of all dependence measures across locations is provided in Table 12. A more comprehensive understanding requires integrating these facets, the results of which we discuss in the next subsection.

City	$\mathcal{H}_{\text{PM}_{2.5};\text{RH}}^R$	$\mathcal{H}_{\text{PM}_{2.5};\text{AT}}^R$	$\mathcal{H}_{\text{PM}_{10};\text{RH}}^R$	$\mathcal{H}_{\text{PM}_{10};\text{AT}}^R$	$\mathcal{H}_{\text{SO}_2;\text{RH}}^R$	$\mathcal{H}_{\text{SO}_2;\text{AT}}^R$	$\mathcal{H}_{\text{NO}_2;\text{RH}}^R$	$\mathcal{H}_{\text{NO}_2;\text{AT}}^R$
AMD	0.963	0.987	0.967	0.990	0.890	0.937	0.891	0.936
BLR	0.989	1.0	0.976	0.992	0.973	0.998	0.974	0.991
CHN	0.952	0.959	0.971	0.972	0.983	0.985	0.953	0.969
DEL	0.887	0.866	1.0	1.0	0.839	0.850	1.0	0.998
HYD	0.955	0.983	0.955	0.985	0.978	0.967	0.972	0.977
KOL	0.972	0.914	0.971	0.922	0.995	0.943	0.993	0.942
MUM	0.958	0.984	0.956	0.990	1.0	0.988	0.975	0.986
AGT	0.916	0.921	0.942	0.935	0.944	0.939	0.946	0.941
ASN	0.855	0.930	0.858	0.933	0.839	0.951	0.848	0.916
BDI	0.902	0.925	0.936	0.972	0.914	0.952	0.943	0.928
BGP	0.934	0.910	0.961	0.962	0.968	0.972	0.905	0.914
BPL	0.933	0.925	0.944	0.961	0.974	0.988	0.940	0.965
BSR	0.918	0.861	0.917	0.889	0.913	0.892	0.847	0.766
BKN	0.896	0.894	0.942	0.972	0.899	0.924	0.941	0.961
GWH	0.923	0.902	0.933	0.921	0.853	0.872	0.725	0.645
IND	0.911	0.956	0.913	0.976	0.896	0.991	0.901	0.978
KOP	0.879	0.971	0.891	0.978	0.577	0.828	0.873	0.973
LKO	0.955	0.967	0.949	0.975	0.958	0.987	0.913	0.949
MAN	0.972	0.990	0.979	0.986	0.938	0.959	0.885	0.936
PDY	0.964	0.954	0.975	0.984	0.986	0.989	0.986	0.936
RPR	0.934	0.970	0.946	0.981	0.910	0.939	0.887	0.943
SXR	0.985	0.969	0.981	0.965	0.956	0.950	0.948	0.923
TVM	0.956	0.930	0.968	0.939	0.878	0.814	0.961	0.943
VTZ	0.944	0.919	0.954	0.940	0.924	0.918	0.949	0.931

**Table 3** Relative conditional entropy  $\mathcal{H}_{X,Y}^R$  for all the pollutant-weather variable pairs across cities. The maximum and minimum values for each pair are highlighted in blue and red, respectively.

### 3.2 Multi-Metric Compound Scoring of Pollutant–Meteorology Correlations

This section presents our key findings of a PCA-based composite assessment of the dependence of pollutants and meteorology variables derived from multiple correlation measures. We first examine intra-city patterns, focusing on the strength of dependence across all pollutant–meteorological variable pairs within individual cities. The analysis is then extended to a cross-city comparison, evaluating variability in composite correlation strength across all variable pairs among different urban locations. Based on the compound correlation score we then classify the cities into different clusters of varying pollutant-weather variables interaction strengths.

#### 3.2.1 Intra-City Correlation Strength for each Pollutant-Weather Variable Pair

At the first level of analysis, we use principal component analysis to quantify the overall strength and structure of correlation between air pollutants and meteorological variables within each city. For a given city, we compute correlation strengths for all the pollutant–weather variable pairs using three distinct statistical metrics<sup>1</sup>, namely,  $|r_{X,Y}|$ ,  $I_{X,Y}$  and  $h_{X,Y}^R$ . Thus, we have a city-specific data matrix of dimension  $8 \times 3$ , where each row corresponds to a particular pollutant–meteorological variable pair, and each column represents one correlation measure.

PCA is applied to the Z-score standardized values of this input matrix to extract the weights  $w_k$  for the three features, i.e., the three correlation

<sup>1</sup>It is to be noted that ignoring the directionality, we consider only the strength of the linear association of the correlation. Also note that, larger  $\mathcal{H}_{X,Y}^R$  indicates weaker interaction and hence taking  $h^R = (1 - \mathcal{H}^R)$  reverses its direction so that all three terms are on the same scale.

measures. These weights are then used to construct the first principal component [see Eq. (11)]. Thus, for the pollutant-weather variable pair  $j = (X, Y)$ , we have,

$$\tilde{\lambda}_{j=(X,Y)} = w_1 |\tilde{r}_{X,Y}| + w_2 \tilde{I}_{X,Y} + w_3 \tilde{h}_{X,Y}^R, \quad (18)$$

where  $|\tilde{r}_{X,Y}|$ ,  $\tilde{I}_{X,Y}$ , and  $\tilde{h}_{X,Y}^R$  denote the Z-score normalized versions of  $|r_{X,Y}|$ ,  $I_{X,Y}$ , and  $h_{X,Y}^R$ , respectively. To convert it into a suitable composite correlation score, we shift the values to a non-negative scale by subtracting the minimum value from all the entries of the PC1 and then dividing by the range of  $\tilde{\lambda}_j$ . Thus, we arrive at a score,

$$\lambda_j = \frac{\tilde{\lambda}_j - \min(\tilde{\lambda}_j)}{\max(\tilde{\lambda}_j) - \min(\tilde{\lambda}_j)} \quad (19)$$

This transformation preserves the relative ranking and can be interpreted as a strength-only measure which is bounded in the range  $[0, 1]$ .

This exercise is repeated for each city. Thus, for the  $i$ -th city, we have an array  $\lambda_j^{(i)}$ , which provides a measure for the overall strength of the  $j$ -th pollutant-weather variable pair. The min-max normalization implies that,  $0 \leq \lambda_j^{(i)} \leq 1$ ; larger value of  $\lambda_j^{(i)}$  implies stronger correlation between the  $j$ -th pair. We refer to  $\lambda_j^{(i)}$  as local correlation score (LCS) for the  $j$ -th variable pair in the  $i$ -th city. For all the cities, the first principal component, in this case, accounts for at least 69% of the total variance. Using Eqs. (10), (11), (18) and (19), we compute the values of local correlation score for inter city pollutant-variable pairs. Table 4 presents the cities for which the LCS values are large ( $> 0.7$ ) for a given variable pair. This intra-city analysis highlights which specific pollutant-meteorological interactions exhibit the strongest and most consistent relationships within each urban environment. Such localized insights are essential for identifying the most influential meteorological drivers of pollutant behavior and can guide city-specific environmental monitoring, forecasting models, or intervention strategies.

Variable Pair	Cities with Very High LCS	No. of Cities
PM <sub>2.5</sub> -RH	MUM (0.930), AMD (0.859), HYD (0.855), KOP (0.739)	4
PM <sub>2.5</sub> -AT	CHN (1), DEL (1), KOL (1), AGT (1), ASN (1), BGP (1), BPL (1), GWH (1), VTZ (1), LKO (0.957), BDI (0.919)	11
PM <sub>10</sub> -RH	AMD (1), BLR (1), HYD (1), MUM (1), BKN (1), KOP (1), IND (0.989), BPL (0.789)	8
PM <sub>10</sub> -AT	GWH (0.974), AGT (0.966), KOL (0.953), CHN (0.942), ASN (0.880), BKN (0.860), LKO (0.802), BDI (0.771)	8
SO <sub>2</sub> -RH	LKO (0.856), GWH (0.823), IND (0.772), MAN (0.725)	4
SO <sub>2</sub> -AT	LKO (1), TVM (1), BDI (0.855)	3
NO <sub>2</sub> -RH	IND (1), MAN (1), RPR (1), BPL (0.942), KOP (0.933), BLR (0.793)	6
NO <sub>2</sub> -AT	BDI (1), BSR (1), PDY (1), SXR (1), BKN (0.729)	5

**Table 4** Cities exhibiting strong pollutant-weather variable pair associations (LCS  $> 0.7$ ), identified via PCA.

### 3.2.2 Comprehensive Correlation Score: Cross-City Aggregation

Building on the intra-city analysis, we next extend the investigation to a cross-city scale, aiming to integrate and compare the strength of various pollutant-meteorology interactions across urban environments.

In this level of analysis, we evaluate the spatial consistency and variability of pollutant-weather interactions by aggregating correlation metrics for each variable pair across all cities. This allows us to assess the extent to which specific pollutant-weather relationships exhibit coherent patterns or divergence across various locations. For each of the pollution-weather variable pairs we compile the corresponding correlation coefficients from all  $m = 24$  cities, using  $p = 3$  distinct correlation measures ( $|\tilde{r}_{X,Y}|$ ,  $\tilde{I}_{X,Y}$  and  $h_{X,Y}^R$ ). This yields a pair specific input matrix of size  $24 \times 3$  where each row represents a city and each column corresponds to a correlation measure. Each column of

the matrix is then standardized via Z-score normalization, followed by PCA. The first principal component loadings are then used to construct the raw spatial correlation score  $\tilde{\phi}_i^{(j)}$  for each variable pair  $j$  across all the cities.

To convert this to a suitable non-negative composite score, we shift each value by subtracting the minimum of the observed values of  $\tilde{\phi}_i$ .

$$\phi_i = \tilde{\phi}_i - \min(\tilde{\phi}_i) \quad (20)$$

This procedure is repeated for all the  $j$  variable pairs ( $\forall j = 1, \dots, 8$ ). Thus, for the  $j$ -th variable pair, we arrive at a spatial correlation score (SCS),  $\phi_i^{(j)}$ , which measures the overall strength of correlation in  $j$ -th pollutant-weather variable pair across all the cities ( $\forall i = 1, \dots, 24$ ). The SCS values corresponding to each city for all the variable pairs are presented in Table 13 in Appendix.

In the next stage of our analysis, we amalgamate the full spectrum of pollutant-weather correlation behavior across cities as well as variable pairs into a single, unified measure. To achieve this, we construct an input matrix of size  $24 \times 8$ , where each entry  $\phi_i^{(j)}$  represents the SCS value for  $i^{\text{th}}$  city and  $j^{\text{th}}$  variable pair. Evidently  $i = 1, 2, 3, \dots, 24$  and  $j = 1, 2, \dots, 8$ . This matrix reflects the complete landscape of localized correlation strengths across all urban environments and variable combinations. After applying Z-score normalization to this matrix, we perform PCA once more and extract the first principal component, which accounts for about 59.42% of total variability. This leads to a total correlation score of the  $i^{\text{th}}$  city,  $\tilde{\mathcal{C}}(i)$ , which is the weighted linear combination of the corresponding SCS values. This is expressed as [see Eq. (11)],

$$\tilde{\mathcal{C}}(i) = \sum_{j=1}^8 w_j \tilde{f}_j(i), \quad (21)$$

where,  $\tilde{f}_j$  corresponds to the standardized value of SCS for the  $j^{\text{th}}$  variable pair, and  $w_j$  refers to the corresponding weight. The numerical values of the PCA loadings are found to be,

$$\begin{aligned} w_1 &= 0.408..., w_2 = 0.310..., w_3 = 0.331..., \\ w_4 &= 0.376..., w_5 = 0.352..., w_6 = 0.318..., \\ w_7 &= 0.358..., w_8 = 0.365... \end{aligned} \quad (22)$$

Cluster	$\mathcal{C}$	Cities	Cluster	$\mathcal{C}$	Cities
I	8.648	ASN	II	6.550	BKN
	7.959	BSR		6.162	GWH
				5.714	KOP
		5.642		BDI	
		4.761		AGT	
III	4.403	IND	IV	2.142	SXR
	4.375	BPL		2.011	LKO
	4.019	RPR		1.696	HYD
	3.632	MAN		1.677	MUM
	3.460	BGP		1.608	DEL
	3.124	KOL		1.554	AMD
	2.651	TVM		0.959	CHN
	2.650	PDY		0	BLR
2.636	VTZ				

**Table 5** Classification of cities based on Comprehensive Correlation Score ( $\mathcal{C}$ ).

and are comparable across all the variable pairs. This observation is consistent with a subsequent PCA-based sensitivity analysis [See Sec. 3.2.3 below].

Once again, we shift the values of the first principal component,

$$\mathcal{C}(i) = \tilde{\mathcal{C}}(i) - \min\{\tilde{\mathcal{C}}(i)\}, \quad (23)$$

to convert it to a non-negative score while preserving the relative ranking. We refer to  $\mathcal{C}(i)$  as Comprehensive Correlation Score (CCS), which serves as a measure of overall pollutant-weather variable correlation strength in the cities.

We apply k-means clustering to categorize cities into distinct groups based on the strength of their CCS ( $\mathcal{C}$ ) values, revealing structural similarities in pollutant-weather interactions. We compute comprehensive correlation score in the cities using Eq. (23) and then based on these score, we apply k-means clustering to categorize them into different groups. This leads to four distinct clusters:

- Cluster I (Very high):  $\mathcal{C} \geq 7.959$
- Cluster II (High):  $4.761 \leq \mathcal{C} \leq 6.550$
- Cluster III (Moderate):  $2.636 \leq \mathcal{C} \leq 4.403$
- Cluster IV (Low):  $\mathcal{C} \leq 2.142$

The cities belonging to these clusters and their corresponding CCS values are summarized in Table 5. This classification which reflects systemic pollutant–weather interaction strength, provides a valuable basis for region-specific environmental modeling, comparative vulnerability assessments, and the design of transferable mitigation strategies tailored to cities with similar correlation dynamics. Fig. 4 depicts the geographic visualization of city clusters of similar correlation strength. We find that most megacities exhibit rel-

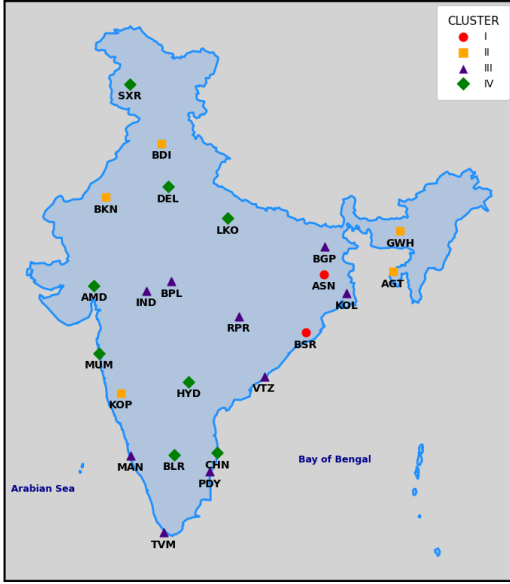


**Fig. 4** Spatial visualization of city clusters according to comprehensive correlation score  $\mathcal{C}$ . The map shows the cities corresponding to very high (red), high (orange), moderate (violet), and low (green) values of  $\mathcal{C}$ .

atively low to moderate total correlation strength, reflecting complex and possibly more heterogeneous pollutant-meteorology interactions. In contrast, cities like Asansol and Bhubaneswar, which are comparatively less populated, show significantly higher correlations, indicating a stronger link between atmospheric conditions and pollutant fluctuations. These findings reveal important spatial variability in pollutant-meteorology dynamics across urban environments and provide a foundation for further theoretical exploration of pollutant-meteorology relationships across diverse spatial scales.

### 3.2.3 Sensitivity Analysis

Sensitivity analysis is used to assess the extent to which individual variable-pairs contribute to the comprehensive correlation score  $\mathcal{C}$ . We have noted that, in the computation of CCS, the first principal component accounts for the maximum variability  $\Sigma = 59.42\%$ , explained by all the variable pairs. Let, the percentage of reduction in variance ( $\Delta\Sigma_j$ ) due to exclusion of the  $j^{\text{th}}$  variable pair be given by,

$$\Delta\Sigma_j(\%) = \frac{\Sigma - \Sigma_j}{\Sigma} \times 100, \quad (24)$$

where,  $\Sigma_j$  denotes the variance accounted for by the first principal component when the  $j^{\text{th}}$  variable pair is excluded and PCA is reapplied to the remaining  $j - 1$  variable pairs. In practice, small values of  $|\Delta\Sigma_j|$ , i.e.,  $\leq 3\%$  are considered negligible, indicating that the PCA structure is robust to the removal of the corresponding variable pair. On the other hand, values exceeding 5% are typically regarded as strong, indicating that the excluded variable pair has a significant effect on the PC1 variance.

Excluded pair	$\Sigma_j$ (%)	$\Delta\Sigma_j$ (%)
PM <sub>2.5</sub> -RH	57.25	-2.17
PM <sub>2.5</sub> -AT	62.36	2.94
PM <sub>10</sub> -RH	61.47	2.05
PM <sub>10</sub> -AT	59.26	-0.16
SO <sub>2</sub> -RH	60.43	1.01
SO <sub>2</sub> -AT	61.92	2.50
NO <sub>2</sub> -RH	60.23	0.80
NO <sub>2</sub> -AT	59.86	0.44

**Table 6** Change in percentage of variance explained for the first principal component upon individual exclusion of each variable pair.

Table 6 presents the results of the sensitivity analysis, which we compute using Eq. (24), showing the variance explained by the first principal component after sequentially excluding each of the eight pollutant–meteorology variable pairs and reapplying PCA on the remaining set. The table also includes the percentage change in explained variance resulting from the exclusion of each pair. The results indicate that the variance loss from removing any one pair is minimal, suggesting that the comprehensive correlation score is robust

and not overly dependent on any specific interaction. This further reinforces the consistency of the combined effect across multiple cities. However, amongst all pairs, PM<sub>2.5</sub>-RH pair appears to be the most influential, with its removal causing a modest decrease of variance (2.17%) whereas interaction pairs like PM<sub>2.5</sub>-AT, SO<sub>2</sub>-AT and PM<sub>10</sub>-RH record a slight increase (almost 2.50%) in explained variance when excluded.

### 3.3 Temporal Correlation

This subsection presents the results of the temporal correlation analysis between pollutants and meteorological variables. Using time-domain measures, we examine the directionality and lead-lag structure of their interactions, highlighting key temporal dependencies that extend beyond static associations.

#### 3.3.1 Transfer Entropy

We compute the transfer entropies,  $\mathcal{T}_{X \rightarrow Y}$  and  $\mathcal{T}_{Y \rightarrow X}$ , using Eq. (15) for all pollutant-weather pairs  $(X, Y)$  in each city. To quantify the dominant direction of information flow, we define  $\Delta\mathcal{T}_{X,Y} = [\mathcal{T}_{X \rightarrow Y} - \mathcal{T}_{Y \rightarrow X}]$ . A positive value ( $\Delta\mathcal{T}_{X,Y} > 0$ ) implies that pollutants ( $X$ ) leads meteorological parameters ( $Y$ ), whereas a negative value ( $\Delta\mathcal{T} < 0$ ) indicates that  $Y$  leads  $X$ . As seen from Table 7,  $\Delta\mathcal{T}_{X,RH} < 0$  for the majority of cities, suggesting that relative humidity (RH) predominantly drives variations in pollutant concentrations. However, a smaller subset of cities, including Delhi, Hyderabad, Bhubaneswar, Guwahati, Lucknow, Mangaluru, Thiruvananthapuram, and Visakhapatnam, exhibits the opposite pattern, where PM<sub>2.5</sub> changes precede those in RH. Similar trends are observed for other pollutant-RH pairs such as (PM<sub>10</sub>, RH), (NO<sub>2</sub>, RH), and (SO<sub>2</sub>, RH), where most cities show RH as the leading variable, though a few instances with  $\Delta\mathcal{T}_{X,RH} > 0$  also occur, as reported in Table 7. Conversely, nearly all cities show  $\Delta\mathcal{T}_{X,AT} > 0$  for pollutant-ambient temperature pairs, indicating that pollutant variations generally precede those in AT. Only a few exceptions with  $\Delta\mathcal{T}_{X,AT} < 0$  are observed. Thus, in most of the locations where RH leads the pollutants, AT tends to lag behind them.

It is noteworthy that the magnitudes of  $\Delta\mathcal{T}$  remain close to zero across most locations, with

the sole exception of Srinagar, Baddi, Asansol and Bikaner likely reflecting its distinct meteorological regime due to geographic factors. All other values are substantially smaller, indicating limited directional asymmetry in information flow. The relatively small values of  $\Delta\mathcal{T}$ , irrespective of the correlation strength between pollutants and weather variables, suggest that neither variable solely governs the underlying dynamics. Instead, the comparable TE magnitudes in both directions across cities indicate a bidirectional relationship between pollutants and meteorological parameters characterized by their mutual influence [61]. This highlights the importance of considering these variable pairs as components of a coupled dynamical system in the study of air quality.

#### 3.3.2 Time-Delayed Mutual Information

We evaluate  $I_{X,Y}(\tau)$  using Eq. (16) for  $\tau \in [-10, 10]$  days, with  $X$  as all four pollutants and  $Y$  as the two weather variables. We find that, for particulate matter-RH pairs [(PM<sub>2.5</sub>, RH) and (PM<sub>10</sub>, RH)], the TDMI curves exhibit a global maximum at zero lag ( $\tau = 0$ ) and subsequently decays to constant values for large positive and negative lags. This behaviour is shown in Fig. 6 (in Appendix) for a few representative cities since most locations exhibit similar behavior for the particulate matter-RH pairs. A comparable trend is also observed for the gaseous pollutant-RH pairs [(NO<sub>2</sub>, RH) and (SO<sub>2</sub>, RH)], though the number of cities displaying this pattern is smaller. In contrast, no consistent or discernible pattern emerges for the pollutant-AT (ambient temperature) pairs. While we analyzed these cases as well, the absence of meaningful structure in their TDMI profiles led us to exclude them from further discussions.

The TDMI analysis for pollutant-RH pairs provides valuable insight into how mutual information evolves over time, revealing the characteristic response timescale of pollutant dynamics to humidity variations. As shown in Fig. 6 (in Appendix), the TDMI decays rapidly and displays an exponential dependence for  $\tau > 0$ . Accordingly, we propose the following form for the decay,

$$\Delta_{X,Y}(\tau) = I_{X,Y}(\tau) - I_{X,Y}^0 \approx ae^{-\tau/\tau_0}, \quad (25)$$

City	$\Delta\mathcal{T}_{(\text{PM}_{2.5},\text{RH})}$	$\Delta\mathcal{T}_{(\text{PM}_{2.5},\text{AT})}$	$\Delta\mathcal{T}_{(\text{PM}_{10},\text{RH})}$	$\Delta\mathcal{T}_{(\text{PM}_{10},\text{AT})}$	$\Delta\mathcal{T}_{(\text{NO}_2,\text{RH})}$	$\Delta\mathcal{T}_{(\text{NO}_2,\text{AT})}$	$\Delta\mathcal{T}_{(\text{SO}_2,\text{RH})}$	$\Delta\mathcal{T}_{(\text{SO}_2,\text{AT})}$
AMD	-0.035	0.006	-0.031	0.017	-0.033	0.023	-0.025	0.002
BLR	-0.007	-0.004	-0.007	0.020	-0.017	0.007	-0.007	0.011
CHN	-0.005	0.009	-0.002	-0.001	-0.003	-0.003	-0.011	0.002
DEL	0.008	0.027	0.008	0.026	-0.001	0.005	0.002	0.006
HYD	0.064	0.071	0.066	0.075	-0.002	0.009	0.005	0.008
KOL	-0.021	0.018	-0.025	0.008	-0.019	0.013	0.001	0.001
MUM	-0.014	0.003	-0.008	0.005	-0.004	0.005	-0.003	0.003
AGT	-0.050	0.060	-0.035	0.055	0.017	0.146	-0.130	-0.052
ASN	-0.078	0.199	-0.163	0.099	-0.154	0.096	-0.011	0.229
BDI	-0.007	0.127	0.063	0.208	0.106	0.317	0.083	0.298
BGP	-0.023	0.067	0.022	0.098	-0.103	-0.015	-0.039	0.018
BPL	-0.036	0.067	0.037	0.112	0.032	0.129	-0.054	0.057
BSR	0.025	0.117	0.055	0.226	-0.073	0.055	-0.063	-0.039
BKN	-0.104	0.112	0.067	0.383	-0.032	0.273	-0.084	0.168
GWH	0.018	0.044	0.040	0.108	-0.001	0.048	-0.056	-0.023
IND	-0.032	0.069	0.125	0.250	0.038	0.167	0.082	0.090
KOP	-0.085	0.021	-0.043	0.083	-0.068	0.049	0.017	0.011
LKO	0.016	0.070	-0.005	0.025	-0.010	0.034	-0.042	0.040
MAN	0.079	0.150	0.093	0.184	0.135	0.097	0.024	0.146
PDY	-0.101	0.072	-0.060	0.163	-0.115	0.043	-0.104	0.066
RPR	-0.057	0.009	0.015	0.092	-0.162	-0.072	-0.040	-0.010
SXR	-0.272	0.026	-0.247	0.045	-0.356	-0.007	-0.171	0.041
TVM	0.009	0.029	0.003	0.002	0.003	-0.030	-0.002	0.026
VTZ	0.048	0.057	0.058	0.118	0.088	0.141	0.004	0.018

**Table 7** Spatial distribution of directional information flow ( $\Delta\mathcal{T}$ ) for pollutant–weather variable pairs. Positive (blue) and negative (red) values are color-coded to indicate the dominant direction of information flow.

which provides a good fit across all pollutant–RH pairs ( $X, Y$ ). Here,  $I_{X,Y}^0$  denotes the saturation value at large positive  $\tau$ ,  $a$  is a constant prefactor and  $\tau_0$  is the typical time-scale of decay. These parameters depend on the city and the variable pair considered.

This exponential decay is illustrated in Fig. 5 where we present a semilog plot of  $\Delta_{X,Y}(\tau)/a$  as a function of the scaled variable  $\tau/\tau_0$  for a set of selected cities for all pollutant–RH pair. This behavior suggests an almost instantaneous adjustment of pollutant concentrations to humidity fluctuations, with the influence of any individual RH perturbation dissipating rapidly—typically within a few days. Such rapid decay indicates limited temporal persistence in pollutant–RH interactions. However, certain cities display TDMI profiles that deviate markedly from this general trend (which are not shown here). In these cases, MI peaks at a nonzero lag (either positive or negative), and the decay deviates noticeably from an exponential form. These features suggest a delayed and more persistent response of fine particulate

levels to humidity changes, likely arising from distinct local meteorological or emission conditions.

## 4 Discussion

Meteorological variables exhibit heterogeneous influences on pollutant concentrations with variation in strength and pollutant types across urban regions. While earlier works [27–29, 62] primarily relied on individual correlation measures, the PCA-based composite index used here provides a robust integration of multiple metrics enabling systematic comparison across locations. This index also supports the classification of urban regions according to the strength of pollutant–meteorology dependence, highlighting distinct groups of cities with relatively strong or weak composite correlations and offering a structured perspective on spatial heterogeneity. Regions with stronger composite dependence are likely dominated by meteorological controls on dispersion, transformation, or accumulation, whereas weaker

dependence may indicate a greater influence of local emission patterns.

The unified correlation strength, transfer entropy, and time-delayed mutual information provide a physically coherent picture of pollutant–meteorology interactions. The composite correlation score developed here identifies where meteorological control is strong, while TE reveals the direction of influence and TDMI characterises the timescales of response. The observed spatial and temporal patterns are consistent with known atmospheric processes governing dispersion, transport, and chemical transformation, lending physical credibility to the information-theoretic framework.

The PCA-based integration of multiple correlation measures advances beyond single-metric approaches. It reduces metric-specific sensitivity and improves interpretability across large multi-city pollutant–meteorology datasets. The resulting classification translates statistical dependence patterns into meaningful spatial groupings, with potential applications in air quality management and comparative assessments.

Several limitations warrant consideration. Using daily-averaged data may blur short-term processes such as diurnal cycles or transient pollution events. The focus on pairwise dependencies does not capture multivariate interactions or nonlinear feedbacks among pollutants and meteorological variables, and seasonal variability is not explicitly addressed. The PCA-based approach, while useful for integration, can lose information from lower-variance but potentially important structures and may under-represent nonlinear behavior. These considerations suggest that PCA-based composites should complement, rather than replace, more detailed process-level analyses.

Despite these limitations, the framework has important implications. The classification of urban regions based on composite dependence strength can inform region-specific air quality management strategies, support comparative assessments across cities, and provide a foundation for integrating meteorological sensitivity into predictive or scenario-based modeling. Overall, the PCA-based composite assessment offers a robust and transferable tool for understanding pollutant–meteorology relationships, advancing both methodological practice and interpretive understanding in multi-city air quality studies.

## 5 Conclusion

Our work contributes to the expanding application of statistical physics and information-theoretic tools to the study of real-world environmental systems. Using entropy-based measures, we analyze both static interdependence and dynamic information flow to investigate correlations, fluctuations, and variability between air pollutants and meteorological variables across multiple Indian cities. By combining both linear and nonlinear dependency measures, namely, Pearson correlation, mutual information, relative conditional entropy, as well as transfer entropy and time-delayed mutual information, we build a comprehensive picture of how environmental variables jointly evolve in urban atmospheres. In the static analysis, to aggregate these diverse correlation patterns, we introduce a multi-level compound measure of pollutant–meteorological correlation strength. Using principal component analysis, we first quantify the intra-city correlation strength (LCS) for each pollutant–weather variable pair, identifying the most dominant interactions within each urban environment. This localized assessment provides valuable insight into the specific meteorological drivers governing pollutant variability, supporting the design of city-specific air quality management and forecasting models. Extending the framework to a cross-city scale, we derive a comprehensive correlation score ( $\mathcal{C}$ ) that enables comparison and ranking of systematic pollutant–meteorology interaction strengths across cities. This comparative amalgamation uncovers notable spatial heterogeneity. Most megacities exhibit relatively low to moderate overall correlations, reflecting complex and heterogeneous atmospheric processes whereas several less populated cities demonstrate markedly stronger pollutant–weather coupling. These contrasts highlight the role of regional climatic regimes, emission characteristics, and urban morphology in shaping local air quality dynamics. Furthermore, PCA-based sensitivity analysis indicates that no single pollutant–weather variable pair exerts a dominant influence, highlighting the multifactorial nature of these interactions. Overall, the proposed multi-metric and multi-scale framework not only advances understanding of pollutant–meteorology relationships but also establishes a quantitative

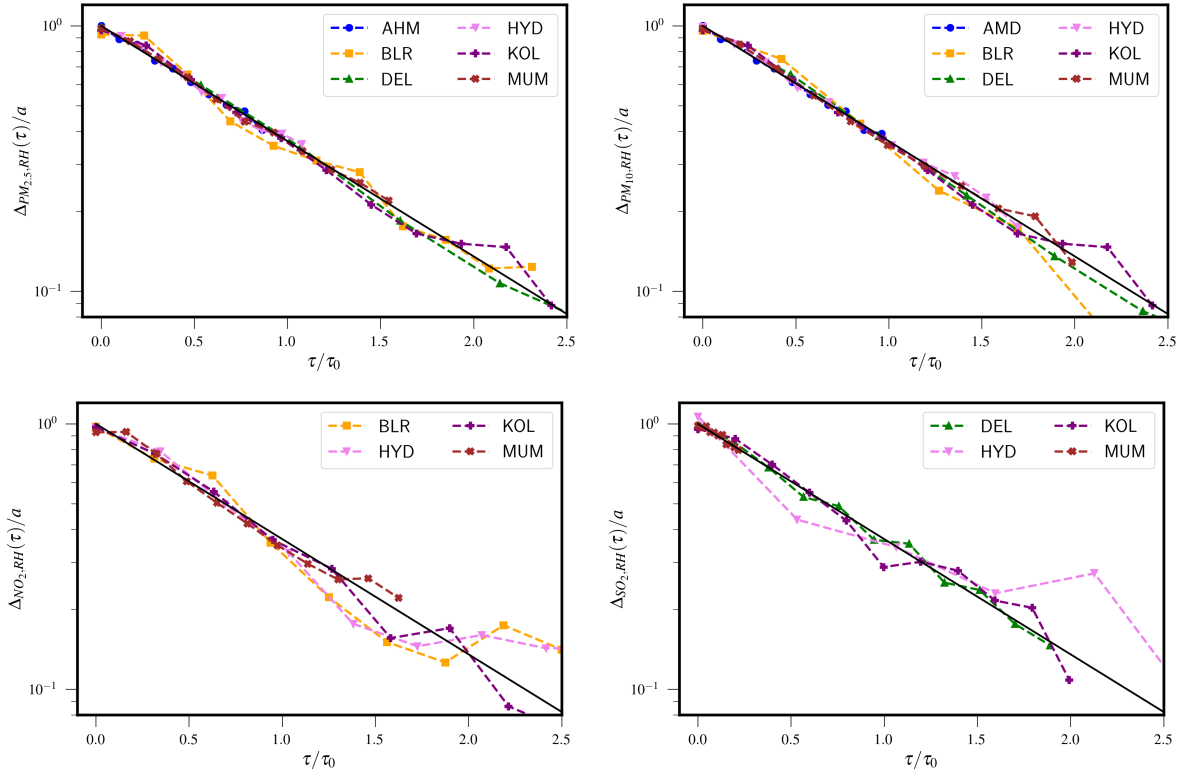


**Fig. 5** Exponential decay for all four pollutant-RH pairs across selected representative cities, plotted on a semi-logarithmic scale with  $\Delta_{X,Y}/a$  as a function of the scaled variable  $\tau/\tau_0$ . In each panel, the black solid line denotes the function  $e^{-\tau/\tau_0}$ .

basis for developing region-specific forecasting models and adaptive mitigation strategies.

We further study the temporal structure of pollutant-weather variable correlations through transfer entropy and time-delayed mutual information. TE analysis of the pollutant-weather variable pairs show that in most locations where RH leads the pollutants, AT tends to lag behind them, highlighting contrasting temporal roles of these meteorological drivers in influencing pollutant dynamics. Although the values of  $\Delta\mathcal{T}$  are very small in several cities showing bidirectional information flow, suggesting feedback mechanisms between pollutant levels and meteorological parameters. The TDMI results further indicate that, in many cases, mutual information peaks at lag zero and decays exponentially with increasing lag, implying predominantly contemporaneous interactions with limited temporal memory, reflecting short-lived correlations. These decay profiles may serve as useful indicators of system responsiveness and reactivity.

More broadly, the integrative entropy-based approach demonstrated here provides a promising foundation for future work incorporating seasonal regimes, multivariate interactions, and nonlinear dynamical modeling. Such extensions may further enhance understanding of urban atmospheric processes and support region-specific mitigation and adaptation strategies.

To the best of our knowledge, this work represents the first attempt in this direction, advancing the understanding of spatiotemporal dependencies in urban air quality and supporting region-specific assessments and monitoring under data-scarce or noisy conditions.

## 6 Acknowledgment

The authors sincerely thank the anonymous Associate Editor of the journal “Stochastic Environmental Research and Risk Assessment” for the thoughtful and constructive feedback provided on an earlier version of this manuscript. All these

comments greatly helped to improve the methodological rigor and overall quality of the study. The authors appreciate the contribution of Moumita De in partial data collection during the initial phase of this work. KG acknowledges the support provided by the Indian Statistical Institute, Kolkata during this project.

## 7 Statements and Declarations

- **Data availability Statement:** All the data used in this work are publicly available [41].
- **Competing Interests:** There are no competing interests to declare.
- **Funding:** No funding information to declare.
- **Author contributions:** Koyena Ghosh contributed to data collection, data curation, analysis, visualization, methodology and writing of the draft. Suchismita Banerjee contributed to data curation, analysis, visualization, methodology and writing of the draft. Urna Basu and Banasri Basu contributed to conceptualization, development of the methodology, analysis, supervision and writing of the draft.

## Appendix

This section presents additional numerical tables and figures containing intermediate results that are used in the analysis of the main text. These tables and figures are provided for completeness and reproducibility. Fig. 6 represents the TDMI curves for all four pollutant-RH pairs for some major cities with  $\tau \in [-10, 10]$ . Table 8 provides a detailed list of the selected Indian cities. Table 9 provides a summary showing the city-level mean and standard deviation of each variable across the selected cities, obtained by averaging station-wise statistics. Table 10 presents the computed self entropy values of all pollutants and meteorological parameters. Further, Table 11 gives the conditional entropy values of each pollutant-weather variable pairs and Table 12 provides the summary statistics for the three correlation metrics used in this study. Spatial Correlation Score (SCS) values of all the variable pairs are presented in Table 13.

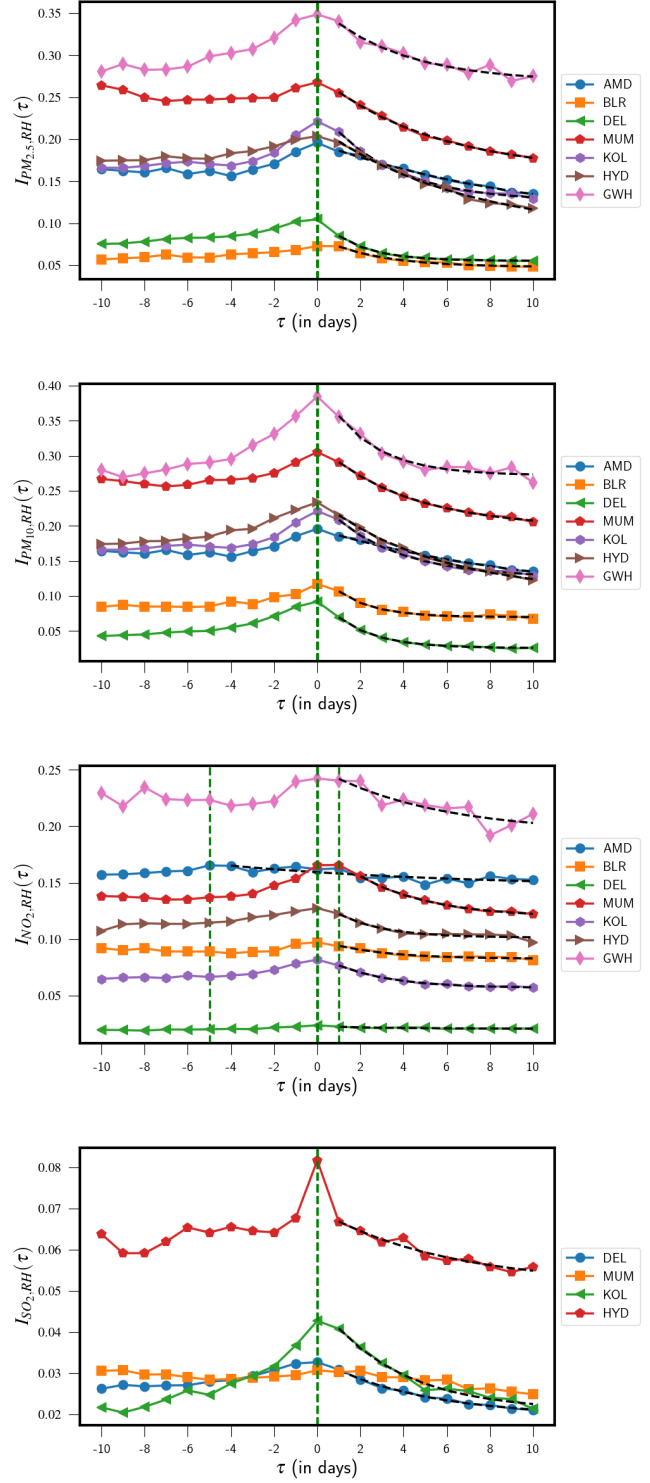


**Fig. 6** TDMI curves for all four pollutant-RH pairs across selected representative cities as a function of time-lag  $\tau$ .

Sl. No.	City	State/ UT	Population (as of 2024)	$N_m$	Analysis period	Latitude, Longitude	Climate zone
1	Ahmedabad (AMD)	Gujarat	90,61,820	3	June 2021 - Dec 2024	23.02°N, 72.57°E	BSh
2	Bengaluru(BLR)	Karnataka	1,43,95,400	5	Jan 2020 - Dec 2024	12.97°N, 77.59°E	Aw
3	Chennai (CHN)	Tamil Nadu	1,23,36,000	7	Jan 2022 - Dec 2024	13.08°N, 80.27°E	As
4	Delhi (DEL)	Delhi NCR	3,46,65,600	23	Jan 2020 - Dec 2024	28.70°N, 77.10°E	Cwa, BSh
5	Hyderabad (HYD)	Andhra Pradesh	1,13,37,900	5	Jan 2020 - Dec 2024	17.39°N, 78.49°E	BSh
6	Kolkata (KOL)	West Bengal	1,58,45,200	7	Jan 2020 - Dec 2024	22.57°N, 88.36°E	Aw
7	Mumbai (MUM)	Maharashtra	2,20,89,000	8	Jan 2020 - Dec 2024	19.08°N, 72.88°E	Aw, Am
8	Agartala (AGT)	Tripura	6,70,388	1	Nov 2020 - Dec 2024	23.83°N, 91.29°E	Aw
9	Asansol (ASN)	West Bengal	15,65,300	1	Sept 2022 - Dec 2024	23.68°N, 86.98°E	Cwa
10	Baddi (BDI)	Himachal Pradesh	29,911	1	Mar 2022 - Dec 2024	30.90°N, 76.80°E	Cwa
11	Bhagalpur (BGP)	Bihar	5,25,429	2	Jan 2022 - Dec 2024	25.25°N, 86.99°E	Cwa
12	Bhopal (BPL)	Madhya Pradesh	26,86,290	3	Feb 2023 - Dec 2024	23.26°N, 77.41°E	Cwa
13	Bhubaneswar (BSR)	Odisha	13,20,910	2	Jan 2024 - Dec 2024	20.30°N, 85.82°E	Aw
14	Bikaner (BKN)	Rajasthan	8,53,869	1	Feb 2023 - Dec 2024	28.02°N, 73.31°E	Bah
15	Guwahati (GWH)	Assam	12,24,170	1	Jan 2020 - Dec 2024	26.14°N, 91.74°E	Cwa
16	Indore (IND)	Madhya Pradesh	34,82,830	1	Jan 2022 - Dec 2024	22.72°N, 75.86°E	Aw
17	Kolhapur (KOP)	Maharashtra	6,69,008	2	Apr 2023 - Dec 2024	16.70°N, 74.24°E	Aw
18	Lucknow (LKO)	Uttar Pradesh	41,32,670	4	Jan 2022 - Dec 2024	26.85°N, 80.95°E	Cwa
19	Mangaluru (MAN)	Karnataka	7,78,685	1	Jul 2021 - Dec 2024	12.91°N, 74.86°E	Am
20	Puducherry (PDY)	Puducherry	9,40,911	1	Jan 2022 - Dec 2024	11.94°N, 79.81°E	Aw
21	Raipur (RPR)	Chhattisgarh	19,23,440	4	Jan 2023 - Dec 2024	21.25°N, 81.63°E	Aw
22	Srinagar (SXR)	Jammu and Kashmir	17,77,610	1	Jan 2022 - Dec 2024	34.08°N, 74.80°E	Cfa
23	Thiruvananthapuram (TVM)	Kerala	30,72,530	2	Jan 2020 - Dec 2024	8.52°N, 76.94°E	Am
24	Visakhapatnam (VTZ)	Andhra Pradesh	10,63,178	1	Jan 2020 - Dec 2024	17.69°N, 83.22°E	Aw

**Table 8** List of selected Indian cities and their geographic, climatic, and demographic characteristics.  $N_m$  denotes the number of monitoring stations in each city with a total of 87 stations across all cities.

City	PM <sub>2.5</sub>		PM <sub>10</sub>		SO <sub>2</sub>		NO <sub>2</sub>		RH		AT	
	$\langle\rho\rangle$	$\sigma$										
AMD	50.451	25.937	108.341	49.491	16.836	12.218	26.839	23.077	51.649	20.786	27.655	4.608
BLR	32.182	28.276	69.397	33.260	6.950	3.430	19.852	12.947	65.252	13.230	24.376	2.274
CHN	29.065	18.996	65.062	34.739	7.421	6.912	17.663	9.754	77.079	7.128	28.994	2.453
DEL	106.634	87.647	214.855	124.326	11.807	7.824	42.046	23.560	62.009	14.335	25.612	7.665
HYD	37.905	21.383	88.143	44.705	9.286	6.913	28.434	16.597	65.973	13.759	26.706	3.511
KOL	49.401	38.823	98.733	68.962	10.220	7.430	25.285	20.820	79.045	14.362	27.353	4.296
MUM	37.464	27.987	100.048	62.168	16.142	14.158	22.151	17.368	78.194	12.886	28.151	3.305
AGT	50.704	38.523	83.383	54.876	24.517	25.379	10.205	6.685	53.025	10.881	22.940	6.479
ASN	70.202	37.078	139.422	78.396	10.800	4.364	30.495	9.881	74.619	20.593	27.139	5.072
BDI	63.491	43.555	144.324	66.082	28.282	15.046	20.810	8.599	62.652	21.746	27.312	6.028
BGP	80.130	61.576	157.491	94.522	17.389	12.263	35.829	29.302	68.461	14.559	24.943	6.450
BPL	46.036	31.753	105.769	49.902	14.477	6.943	24.633	12.151	58.056	19.761	25.837	5.199
BSR	45.444	35.457	93.795	58.455	8.964	8.187	12.346	9.207	73.952	12.633	29.173	3.530
BKN	54.362	47.396	179.915	85.029	3.931	2.630	29.765	14.240	48.699	17.526	28.154	6.734
GWH	62.437	49.999	114.506	87.902	15.652	8.097	6.320	7.279	72.468	14.944	26.099	4.683
IND	45.585	26.748	115.525	51.205	14.307	4.921	57.984	24.716	59.077	20.443	25.770	4.572
KOP	38.671	30.063	86.741	53.292	2.420	3.786	18.993	12.605	67.963	11.120	26.888	2.032
LKO	50.752	28.472	104.108	56.409	13.183	5.510	17.068	13.737	67.841	18.040	24.718	6.670
MAN	26.157	16.072	56.569	33.164	14.575	8.730	19.663	19.324	70.974	9.834	28.700	0.820
PDY	23.886	17.123	48.549	22.422	9.529	4.291	10.543	5.066	78.152	5.990	29.501	2.371
RPR	30.792	16.936	77.046	34.212	7.826	4.492	30.220	21.095	63.094	19.594	26.633	4.540
SXR	26.619	16.496	73.758	49.008	15.906	15.432	11.691	8.869	73.028	12.429	7.939	8.690
TVM	24.445	14.112	48.432	20.567	5.874	1.786	12.876	6.880	77.380	9.244	28.186	1.532
VTZ	45.481	26.495	111.910	52.879	11.465	5.288	35.003	12.529	72.655	8.524	28.368	3.579

**Table 9** A summary table showing the mean ( $\langle\rho\rangle$ ) and standard deviation ( $\sigma$ ) of each variable, obtained by averaging station-level statistics for all the selected cities.

City	$S_{PM_{2.5}}$	$S_{PM_{10}}$	$S_{SO_2}$	$S_{NO_2}$	$S_{RH}$	$S_{AT}$	City	$S_{PM_{2.5}}$	$S_{PM_{10}}$	$S_{SO_2}$	$S_{NO_2}$	$S_{RH}$	$S_{AT}$
AMD	4.533	5.259	3.708	4.149	4.394	2.941	BSR	4.547	5.217	3.002	3.335	3.903	2.628
BLR	4.167	4.888	2.477	3.801	3.987	2.205	BKN	4.739	5.782	2.133	3.956	4.201	3.231
CHN	4.204	4.849	2.854	3.696	3.531	2.350	GWH	4.937	5.492	3.380	2.677	3.918	2.873
DEL	6.158	5.603	3.861	4.459	4.066	3.338	IND	4.397	5.256	2.856	4.506	4.253	2.925
HYD	4.336	5.120	2.932	4.215	4.039	2.695	KOP	4.487	5.227	1.776	3.762	3.622	2.109
KOL	4.745	5.368	2.951	4.083	3.925	2.799	LKO	4.680	5.378	3.258	3.658	4.207	3.285
MUM	4.465	5.399	3.629	4.016	3.860	2.636	MAN	4.021	4.739	3.241	3.745	3.113	0.546
AGT	4.631	5.091	3.835	3.128	3.784	3.163	PDY	3.911	4.430	2.739	2.892	3.202	2.235
ASN	4.866	5.607	2.739	3.591	3.927	2.994	RPR	4.209	5.027	2.878	4.219	4.291	2.953
BDI	4.809	5.509	3.950	3.465	4.271	3.065	SXR	3.918	4.967	3.561	3.273	3.906	3.248
BGP	5.178	5.825	3.573	4.337	3.998	3.264	TVM	3.972	4.490	2.462	3.176	3.670	2.217
BPL	4.565	5.246	3.360	3.884	4.287	3.047	VTZ	4.558	5.301	2.922	3.908	3.364	2.688

**Table 10** Self-entropy values of the selected parameters across cities, highlighting maximum (blue) and minimum (red) values of each variable.

City	$\mathcal{H}_{\text{PM}_{2.5};\text{RH}}$	$\mathcal{H}_{\text{PM}_{2.5};\text{AT}}$	$\mathcal{H}_{\text{PM}_{10};\text{RH}}$	$\mathcal{H}_{\text{PM}_{10};\text{AT}}$	$\mathcal{H}_{\text{SO}_2;\text{RH}}$	$\mathcal{H}_{\text{SO}_2;\text{AT}}$	$\mathcal{H}_{\text{NO}_2;\text{RH}}$	$\mathcal{H}_{\text{NO}_2;\text{AT}}$
AMD	4.364	4.476	5.083	5.204	3.301	3.476	3.696	3.884
BLR	4.122	4.212	4.771	4.847	2.411	2.471	3.702	3.765
CHN	4.001	4.033	4.706	4.713	2.805	2.811	3.522	3.582
DEL	5.464	5.335	6.052	6.016	3.240	3.283	4.502	4.452
HYD	4.142	4.264	4.890	5.045	2.867	2.836	4.096	4.119
KOL	4.610	4.336	5.213	4.948	2.936	2.784	4.054	3.848
MUM	4.278	4.393	5.160	5.347	3.639	3.585	3.915	3.960
AGT	4.244	4.265	4.796	4.760	3.620	3.602	2.960	2.945
ASN	4.158	4.524	4.812	5.233	2.297	2.604	3.045	3.289
BDI	4.339	4.449	5.158	5.356	3.612	3.762	3.269	3.216
BGP	4.836	4.713	5.595	5.601	3.459	3.474	3.923	3.962
BPL	4.259	4.224	4.950	5.044	3.273	3.321	3.650	3.747
BSR	4.173	3.917	4.784	4.637	2.738	2.677	2.825	2.555
BKN	4.248	4.235	5.448	5.621	1.917	1.970	3.724	3.803
GWH	4.559	4.454	5.124	5.058	2.883	2.946	1.942	1.728
IND	4.007	4.205	4.801	5.128	2.56	2.830	4.059	4.407
KOP	3.945	4.355	4.656	5.112	1.025	1.471	3.284	3.660
LKO	4.468	4.527	5.106	5.246	3.121	3.215	3.339	3.473
MAN	3.909	3.980	4.641	4.673	3.040	3.108	3.313	3.504
PDY	3.771	3.731	4.319	4.359	2.702	2.709	2.852	2.707
RPR	3.930	4.082	4.756	4.929	2.618	2.702	3.741	3.978
SXR	3.860	3.795	4.871	4.792	3.406	3.382	3.104	3.021
TVM	3.797	3.695	4.347	4.217	2.161	2.003	3.052	2.994
VTZ	4.305	4.191	5.056	4.981	2.700	2.683	3.710	3.637

**Table 11** City-wise conditional entropy values of air pollutants with respect to meteorological parameters highlighting maximum (blue) and minimum (red) values.

pollutant– weather variable pairs	Pearson correlation ( $r_{X,Y}$ )			Mutual information ( $I_{X,Y}$ )		Relative conditional entropy ( $\mathcal{H}_{X,Y}^R$ )	
	% of cities with $r_{X,Y} < 0$	Median	$\sigma$	Median	$\sigma$	Median	$\sigma$
PM <sub>2.5</sub> -RH	75.00	-0.130	0.182	0.249	0.137	0.939	0.034
PM <sub>2.5</sub> -AT	79.17	-0.300	0.243	0.247	0.181	0.942	0.039
PM <sub>10</sub> -RH	95.83	-0.285	0.207	0.301	0.163	0.955	0.039
PM <sub>10</sub> -AT	87.50	-0.210	0.234	0.281	0.164	0.972	0.035
SO <sub>2</sub> -RH	83.33	-0.140	0.217	0.213	0.147	0.931	0.085
SO <sub>2</sub> -AT	87.50	0.000	0.215	0.190	0.168	0.951	0.052
NO <sub>2</sub> -RH	66.67	-0.195	0.212	0.229	0.156	0.942	0.060
NO <sub>2</sub> -AT	58.33	-0.180	0.226	0.268	0.183	0.943	0.074

**Table 12** Summary statistics of the correlation metrics – Pearson correlation, mutual information, and relative conditional entropy for pollutant–meteorological variable pairs across all cities.

City	$\phi_{PM_{2.5},RH}$	$\phi_{PM_{2.5},AT}$	$\phi_{PM_{10},RH}$	$\phi_{PM_{10},AT}$	$\phi_{SO_2,RH}$	$\phi_{SO_2,AT}$	$\phi_{NO_2,RH}$	$\phi_{NO_2,AT}$
AMD	1.18	1.09	2.83	0.55	1.18	0.58	1.89	0.58
BLR	0	0	2.40	0.05	0.41	0	1.00	0
CHN	0.58	1.77	1.60	0.95	0.43	1.27	0.61	0.61
DEL	2.23	4.37	0	0	2.40	0.38	0	1.04
HYD	1.61	0.96	3.71	0.04	0.80	1.44	1.41	0.47
KOL	1.35	3.59	3.34	3.33	1.61	1.05	1.04	1.32
MUM	2.07	1.05	4.14	0.28	0	0.16	2.08	0.56
AGT	3.03	3.47	3.03	3.42	1.82	3.45	2.04	2.24
ASN	5.60	4.30	6.31	4.38	4.93	3.84	4.37	3.64
BDI	2.94	4.36	3.38	2.69	2.24	4.47	2.13	4.00
BGP	1.97	4.43	3.04	2.35	1.01	0.80	2.24	2.10
BPL	2.46	3.82	4.14	2.47	1.69	0.95	3.48	2.26
BSR	3.73	6.22	4.82	5.53	2.59	2.48	3.89	6.30
BKN	3.95	4.87	5.42	3.00	2.78	3.50	3.47	2.75
GWH	2.60	4.30	3.56	3.81	3.78	2.74	3.30	4.11
IND	2.46	2.26	5.22	1.20	3.33	1.23	3.91	1.41
KOP	4.64	1.09	6.51	1.06	5.18	1.10	4.97	0.82
LKO	0.93	2.16	3.13	1.25	1.25	0.80	1.62	0.87
MAN	1.43	0.86	2.69	0.68	3.56	2.97	3.40	2.12
PDY	0.98	2.25	3.07	0.81	1.83	2.15	0.87	2.57
RPR	2.27	1.78	3.93	1.31	2.73	2.53	3.68	1.12
SXR	0.73	1.33	1.98	1.23	1.10	1.74	1.69	2.49
TVM	1.40	2.19	2.79	1.98	1.66	2.89	0.66	0.81
VTZ	1.52	3.35	2.66	2.00	1.54	0.93	1.39	1.15

**Table 13** SCS ( $\phi$ ) values for 8 pollutant-weather variable pairs across 24 cities. The highest  $\phi$  values for each interaction pair are highlighted with blue color.

## References

- [1] World Health Organization: WHO Global Air Quality Guidelines: Particulate Matter (PM<sub>2.5</sub> and PM<sub>10</sub>), Ozone, Nitrogen Dioxide, Sulfur Dioxide and Carbon Monoxide. World Health Organization, Geneva (2021). <https://www.who.int/publications/item/9789240034228>
- [2] Cencini, M., Cecconi, F., Vulpiani, A.: Chaos: From Simple Models to Complex Systems. World Scientific, Singapore (2010). <https://doi.org/10.1142/7351>
- [3] Baklanov, A., Hänninen, O., Slørdal, L.H., Kukkonen, J., Bjergene, N., Fay, B., Finardi, S., Hoe, S., Jantunen, M., Karppinen, A., *et al.* Atmospheric Chemistry and Physics **7**, 855 (2007) <https://doi.org/10.5194/acp-7-855-2007>
- [4] Nicolis, G., Prigogine, I.: Self-Organization in Nonequilibrium Systems: From Dissipative Structures to Order Through Fluctuations. Wiley, New York (1977)
- [5] Lovejoy, S. Geophysical Research Letters **42**, 7148 (2015) <https://doi.org/10.1002/2015GL065665>
- [6] Lovejoy, S., Schertzer, D.: The Weather and Climate: Emergent Laws and Multifractal Cascades. Cambridge University Press, Cambridge (2013). <https://doi.org/10.1017/CBO9781139093811>
- [7] Runge, J., Bathiany, S., Bollt, E., Camps-Valls, G., Coumou, D., Deyle, E., Glymour, C., Kretschmer, M., Mahecha, M.D., Muñoz-Marí, J., *et al.* Nature Communications **10**, 2553 (2019) <https://doi.org/10.1038/s41467-019-10105-3>
- [8] Seinfeld, J.H., Pandis, S.N.: Atmospheric Chemistry and Physics: From Air Pollution to Climate Change. John Wiley & Sons, New Jersey (2016)
- [9] Jacob, D.J.: Introduction to Atmospheric Chemistry. Princeton university press, USA (1999)
- [10] Wan, Z., Wei, K., Xia, Y.A. Stoch Environ Res Risk Assess **38**, 4243 (2024) <https://doi.org/10.1007/s00477-024-02801-4>
- [11] Antoniadou, N., Stockmarr, A., Pedersen, J.W., *et al.* Stoch Environ Res Risk Assess **39**, 4125 (2025) <https://doi.org/10.1007/s00477-025-03054-5>
- [12] Raga, G.B., Le Moyne, L. Atmospheric Environment **30**, 3987 (1996) [https://doi.org/10.1016/1352-2310\(96\)00122-7](https://doi.org/10.1016/1352-2310(96)00122-7)
- [13] Yu, H.-L., Lin, Y.-C., Sivakumar, B., Kuo, Y.-M. Atmospheric Environment **69**, 37 (2013) <https://doi.org/10.1016/j.atmosenv.2012.10.067>
- [14] Golan, A., Harte, J. Proceedings of the National Academy of Sciences **119**, 2119089119 (2022) <https://doi.org/10.1073/pnas.2119089119>
- [15] Zhao, B., Wang, S., Ding, D., Wu, W., Chang, X., Wang, J., Xing, J., Jang, C., Fu, J.S., Zhu, Y., *et al.* Science of The Total Environment **661**, 375 (2019) <https://doi.org/10.1016/j.scitotenv.2019.01.169>
- [16] Im, U., Geels, C., Hanninen, R., Kukkonen, J., Rao, S., Ruuhela, R., Sofiev, M., Schaller, N., Hodnebrog, Ø., Sillmann, J., *et al.* Frontiers in Environmental Science **10**, 954045 (2022) <https://doi.org/10.3389/fenvs.2022.954045>
- [17] Lin, Y.-C., Lai, C.-Y., Chu, C.-P. Environmental Research **194**, 110693 (2021) <https://doi.org/10.1016/j.envres.2020.110693>
- [18] Cover, T.M., Thomas, J.A.: Elements of Information Theory. John Wiley & Sons, New Jersey (2005). <https://doi.org/10.1002/047174882X>
- [19] Sánchez-Ccoyllo, O., Fatima Andrade, M. Environmental Pollution **116**, 257 (2002) [https://doi.org/10.1016/S0269-7491\(01\)00129-4](https://doi.org/10.1016/S0269-7491(01)00129-4)
- [20] Rowland, O.E. Discover Environment **2**, 75 (2024) <https://doi.org/10.1007/>

s44274-024-00060-2

- [21] Nakyai, T., Santasnachok, M., Thetkathuek, A., Phatrabuddha, N. *Environmental Advances* **19**, 100608 (2025) <https://doi.org/10.1016/j.envadv.2024.100608>
- [22] Malhotra, M., Aulakh, I.K., Gupta, M., Monika, vol. 2768, p. 020033 (2023). <https://doi.org/10.1063/5.0148966>
- [23] Bose, A., Roy Chowdhury, I. *Modeling Earth Systems and Environment* **9**, 2877–2892 (2023) <https://doi.org/10.1007/s40808-022-01670-6>
- [24] Pawar, B.D., Garg, L., Caruana, R.J., Buttigieg, S.C., Calleja, N. *Environment Pollution and Climate Change* **7**, 327 (2023)
- [25] Wang, Q., Li, X. *Journal of Physics: Conference Series* **2168**, 012028 (2022) <https://doi.org/10.1088/1742-6596/2168/1/012028>
- [26] Garsa, K., Khan, A.A., Jindal, P., Middey, A., Luqman, N., Mohanty, H., Tiwari, S. *Environmental Monitoring and Assessment* **195**, 1315 (2023) <https://doi.org/10.1007/s10661-023-11922-2>
- [27] Gupta, S.K., Elumalai, S.P. *Archives of Environmental Contamination and Toxicology* **76**, 572 (2019) <https://doi.org/10.1007/s00244-019-00616-x>
- [28] Maltare, N.N., Vahora, S., Jani, K. *Journal of Cleaner Production* **436**, 140514 (2024) <https://doi.org/10.1016/j.jclepro.2023.140514>
- [29] Oji, S., Adamu, H. *Journal of Air Pollution and Health* **5**, 11 (2020) <https://doi.org/10.18502/japh.v5i1.2856>
- [30] Amoretti, A., Brattan, D.K., Martinoia, L., Matthaiakakis, I. *Physical Review D* **108**, 056003 (2023) <https://doi.org/10.1103/PhysRevD.108.056003>
- [31] Shannon, C.E. *The Bell System Technical Journal* **27**, 379 (1948) <https://doi.org/10.1002/j.1538-7305.1948.tb01338.x>
- [32] Fraser, A.M., Swinney, H.L. *Physical Review A* **33**, 1134 (1986) <https://doi.org/10.1103/PhysRevA.33.1134>
- [33] Steuer, R., Kurths, J., Daub, C.O., Weise, J., Selbig, J. *Bioinformatics* **18**, 231 (2002) [https://doi.org/10.1093/bioinformatics/18.suppl\\_2.S231](https://doi.org/10.1093/bioinformatics/18.suppl_2.S231)
- [34] Schreiber, T. *Physical Review Letters* **85**, 461 (2000) <https://doi.org/10.1103/PhysRevLett.85.461>
- [35] Lelieveld, J., Evans, J.S., Fnais, M., Gianadadaki, D., Pozzer, A. *Nature* **525**, 367 (2015) <https://doi.org/10.1038/nature15371>
- [36] Cohen, A.J., Brauer, M., Burnett, R., Anderson, H.R., Frostad, J., Estep, K., Balakrishnan, K., Brunekreef, B., Dandona, L., Dandona, R., *et al.* *The Lancet* **389**, 1907 (2017) [https://doi.org/10.1016/S0140-6736\(17\)30505-6](https://doi.org/10.1016/S0140-6736(17)30505-6)
- [37] Pompe, B., Runge, J. *Physical Review E* **83**, 051122 (2011) <https://doi.org/10.1103/PhysRevE.83.051122>
- [38] Barnett, L., Barrett, A.B., Seth, A.K. *Physical Review Letters* **103**, 238701 (2009) <https://doi.org/10.1103/PhysRevLett.103.238701>
- [39] Jolliffe, I.T., Cadima, J. *Philosophical transactions of the royal society A: Mathematical, Physical and Engineering Sciences* **374**, 20150202 (2016) <https://doi.org/10.1098/rsta.2015.0202>
- [40] Bro, R., Smilde, A.K. *Analytical methods* **6**, 2812–2831 (2014) <https://doi.org/10.1039/C3AY41907J>
- [41] <https://cpcb.nic.in/namp-data/>
- [42] [https://en.wikipedia.org/wiki/Classification\\_of\\_Indian\\_cities](https://en.wikipedia.org/wiki/Classification_of_Indian_cities)
- [43] <https://www.latlong.net/>
- [44] <https://koppen.earth/>
- [45] <https://worldpopulationreview.com/cities/india>

- [46] Hänel, G. *Advances in Geophysics*, vol. 19, p. 73. Elsevier (1976). [https://doi.org/10.1016/S0065-2687\(08\)60142-9](https://doi.org/10.1016/S0065-2687(08)60142-9)
- [47] Vaishali, Verma, G., Das, R.M. *MAPAN* **38**, 759 (2023) <https://doi.org/10.1007/s12647-023-00656-8>
- [48] Kalman, R.E. *Journal of Basic Engineering* **82**, 35 (1960) <https://doi.org/10.1115/1.3662552>
- [49] Becker, A.: Kalman Filter from the Ground Up. KalmanFilter.NET, (2023). <https://www.kalmanfilter.net/book.html>
- [50] Ferreira, G., Mateu, J., Porcu, E. *Stoch Environ Res Risk Assess* **36**, 4337 (2022) <https://doi.org/10.1007/s00477-022-02266-3>
- [51] Joel, L.O., Doorsamy, W., Paul, B.S. *International Journal of Data Science and Analytics*, 1 (2025) <https://doi.org/10.1007/s41060-025-00825-9>
- [52] Watson, G.S. *Sankhyā: The Indian Journal of Statistics, Series A*, 359–372 (1964)
- [53] Nadaraya, E.A. *Theory of Probability & Its Applications* **9**, 141 (1964) <https://doi.org/10.1137/1109020>
- [54] Bierens, H.J.: *Topics in Advanced Econometrics: Estimation, Testing, and Specification of Cross-section and Time Series Models*. Cambridge University Press, Cambridge (1994)
- [55] Gun, A.M., Gupta, M.K., Dasgupta, B.: *Fundamentals Of Statistics*. World Press, Kolkata (2008)
- [56] Kraskov, A., Stögbauer, H., Grassberger, P. *Physical Review E* **69**, 066138 (2004) <https://doi.org/10.1103/PhysRevE.69.066138>
- [57] Jolliffe, I., p. 1094. Springer, Berlin, Heidelberg (2011). [https://doi.org/10.1007/978-3-642-04898-2\\_455](https://doi.org/10.1007/978-3-642-04898-2_455)
- [58] Tanaka, Y., Mori, Y. *American Journal of Mathematical and Management Sciences* **17**, 61 (1997) <https://doi.org/10.1080/01966324.1997.10737430>
- [59] Tanaka, Y. *Communications in Statistics - Theory and Methods* **17**, 3157 (1988) <https://doi.org/10.1080/03610928808829796>
- [60] Vicente, R., Wibral, M., Lindner, M., Pipa, G. *Journal of computational neuroscience* **30**, 45 (2011) <https://doi.org/10.1007/s10827-010-0262-3>
- [61] Chen, Z., Cai, J., Gao, B., Xu, B., Dai, S., He, B., Xie, X. *Scientific Reports* **7**, 40735 (2017) <https://doi.org/10.1038/srep40735>
- [62] Ulpiani, G., Hart, M.A., Di Virgilio, G., Maharaj, A.M. *Sustainable Cities and Society* **77**, 103553 (2022) <https://doi.org/10.1016/j.scs.2021.103553>